Ben-Gurion University of the Negev

Faculty of Natural Sciences

Computer Science Department

LARGE SCALE SELF-ORGANIZATION IN SIMULATED ACTIN/MYOSIN SYSTEMS

Thesis submitted as part of the requirements

for the M.Sc. degree of Ben-Gurion University of the Negev

Daniel Gordon

August 2009

Subject: Large Scale Self-Organization in Simulated Actin/Myosin Systems

Written By: Daniel Gordon

Advisor 1: Dr. Chen Keaser

Advisor 2: Dr. Oded Farago

Department: Computer Science

Faculty: Natural Sciences

Ben-Gurion University of the Negev

Signatures:

Author: Daniel Gordon	Date
Advisor 1: Dr. Chen Keaser	Date
Advisor 2: Dr. Oded Farago	Date
Dept. Committee Chairman	Date

Abstract

Living cells need to impose inner order, transport organelles from site to site inside the cell, withstand external pressures and propagate themselves to different locations. All of these mechanical needs are supplied by the cells cytoskeleton. One of the components of the cytoskeleton is filamentous actin (F-actin). The two ends of F-actin are distinctly different, making it a polar rod with a ”plus end” and a ”minus end”. Actin defines and preserves the cells shape and allows for cell motion. Actin in the cell has many accessory proteins. One of the more interesting ones is Myosin II, a molecular motor which can convert chemical energy into mechanical work and progress along F-actin towards its plus end. These motors can aggregate and move along more than one filament simultaneously, causing their relative movement.

In-vitro experiments have shown that mixtures of F-actin and myosin II motors can generate different patterns, including bundles, asters, and networks. The dynamics allowing this organization are not yet fully understood. In this work, we present a coarse-grained molecular model for systems consisting of myosin II motors and actin filaments. Within this model, the filaments are represented as flexible rods while the motors are modeled as ”mechanical units” that can bind to, exert forces, and move along the filaments. Thus, the approach balances the need for molecular details with computational simplicity in a manner that allows for simulations which mimic *in-vitro* experiments. We use the model to study, by means of molecular dynamics simulations, the self-organization behavior of the system. Our simulations reveal a very rich phase behavior with several steady-states (different types of bundles and asters both isolated and interconnected) and different global layouts of filaments and motors determined by the length of the filaments and the number of motors per filament, some of which have been observed experimentally. They also provide a visualization of the dynamics leading to these structures and shed light on the role played by the myosin II motors as active linkers which can bind to several filaments and (due to their non-processive nature) switch between them.

Acknowledgments

My field of research was inter-disciplinary demanding much knowledge in many different fields. Without help from people experts in these different fields no progress could have been made. First, Dr. Oded Farago my supervisor from the department of Biomedical Engineering, who encouraged, advised, and listened to my ideas through out my research and who defined the model to be used for building the simulation. My second supervisor Dr. Chen Keasar from the department of Computer Science taught me much in program design and in critical thought, while having much patience to hear my suggestions and different hypotheses, and giving me a free hand to go my own way. Dr. Anne Bernheim from the department of Chemical Engineering, gave invaluable insight into the behavior of actin-myosin systems as perceived in *in-vitro* experiments.

I would also like to thank my wife for her love, advice and patience, and for looking after our lovely children while I worked.

Contents

List of Figures

List of Tables

Chapter 1

Introduction

Living cells need to impose inner order, transport organelles from site to site, withstand external pressures and propagate themselves to different locations. All of these mechanical needs are supplied by the cells cytoskeleton [1]. The cytoskeleton has three main members: microtubules (MT) built from tubulin, actin filaments (F-actin) built from globular actin (G-actin) and intermediate filaments. Defining the mechanical function of each cytoskeleton component coarsely: MT's enable intracellular transport, actin defines and preserves the cells shape and allows for cell motion, and intermediate filaments provide mechanical strength and resistance to shear stress [2]. The dynamic aspects of the cytoskeletons functions are achieved by their ability to polymerize and depolymerize (treadmilling) and by the action of molecular motors, which are specialized proteins that convert chemical energy (e.g., ATP hydrolysis) into mechanical work. This energy is used to fuel the motion of motors along the filaments, allowing intracellular transportation and cell motion.

MTs and actin filaments are polar; the two ends of each of their building blocks (tubulin and G-actin) are distinctly different, and in the filament they are connected head to tail, defining the directionality of the filament. The direction in which the motors propagate along the filament varies from motor to motor. Myosin II motors, for example, "walk" towards the so called plus-end of actin filaments, while myosin VI move in the opposite direction towards the minus-end [3, 4]. Actin filaments serve as the building blocks for larger structures in the cell. These large constructions include networks and bundles which are formed when filaments are cross-linked to each other [5, 6, 7, 8]. The cross-linking of actin filaments can be achieved by actin binding proteins, such as fascin (that binds filaments in a parallel manner) and spectrin (that creates a web like structure), which are static linkers. Motors can also serve as linkers [9], although not static but dynamic. Muscle

cells, for example, consist of contractile bundles which are formed by the association of actin filaments through both static linkers and myosin II motors.

Many experiments have been conducted on the cytoskeleton leading to a better understanding of the biological functions of the cytoskeleton, its mechanical properties, and its biochemical regulation inside the cell [10, 11]. Another aspect which has also been examined in these experiments is the ability of the cytoskeleton to self-organize under the action of the associated motors. Because of the complexity of the self-organization process and due to the large number of cellular components which may be involved, these experiments are done *in-vitro* where parts of the system can be isolated and the major participants can be identified. Introducing only filaments, motors and ATP, different cytoskeleton patterns have been experimentally observed over the past years[12, 13, 9, 14], including asters (star like shapes with filaments plus ends bound by motors at the center of the "star" and the filaments radiate outwards), vortices, rings, networks and bundles. All these phenomena occur in the presence of molecular motors and ATP. The motors produce the forces that change the shape of the system. Self organization occurs only in the presence of multi-headed motor units (mini-filaments), in contrast to single motor proteins which can bind to only one filament, and therefore cannot create relative motion. [15]. The minimal requirement for relative movement is two independent units, each able to connect to a different filament with at least one of them active (able to propagate along a filament). The contraction and relaxation of the sarcomeres in muscle cells, for instance, is achieved by mini-filaments of myosin II motors, each of which consists of about 300 myosin heads.

Actin filaments and MT's form different meta-structures in the cell. Actin is known to create bundles and gel-like networks which are mainly located beneath the cell cortex. MTs usually remain as single long rods, most of which are nucleated in and grow out from centrosomes to form aster-like structures [1]. Asters have also been observed in controlled self organization experiments with both actin and MTs. However the formation of networks has been reported only in experiments with actin, while spirals have been observed only with MTs. The fact that these two systems exhibit some different structural patterns is not surprising given the very different elastic properties of actin and MTs. MTs are stiff with a persistence length [1] on the order of a mm while F-actin is much more flexible with a persistence length of only a few μm [16, 17] Another possible reason for the differences

[1]Persistence length measures the distance along a filament after which the tangent vectors of two points become uncorrelated[2]. This means a filament with a length much shorter than its persistence length will be quite straight, while a filament longer than its persistence length will have more convoluted shapes.

in the *in vitro* self-organization behavior of these systems is the difference in the motors which drive the process. Kinesin and dynein, which connect to MTs, are processive motors. This means that once a motor is connected to a MT, it progresses along it and only rarely disconnects before reaching its destination. On the other hand myosin II, which binds to F-actin, is a non-processive motor, that spends only a short time traveling on the filament before disconnecting from it. This difference in processivity leads to systems with rather different dynamics. Processive motors move smoothly along their filaments, while non-processive motors progress in a stochastic, noisy, manner. The difference in processivity also seems to be the reason why non-processive motors are usually found in aggregates of many motors., while processive motors usually act individually or in small groups. In large aggregates non-processive motors become effectively processive, because the probability of having at least one motor head connected to the filament is high[18]. Differences in processivity and aggregate size also give rise to a difference in the speed of progression. Non-processive aggregates of motors move faster, as each motor head pushes the motor forward and then disconnects allowing other motor heads to connect to the filament. In contrast, processive motors stay connected to the filament, preventing the access of other motors to the same site. *In-vitro* experiments show that kinesin proceeds at a speed of about $0.8\mu ms^{-1}$ whereas myosin II, with approximately 100 heads, proceeds at a speed of $8\mu ms^{-1}$[18].

Self organization of motors-filaments systems has been studied using different theoretical approaches. As these systems are structurally very complex, it is impossible to model them in full atomistic detail. The existing models, therefore, are based on phenomenological, coarse-grained, descriptions which address the problem on larger length- and time-scales. In these coarse-grained (CG) models, the interactions between the motors and the filaments are represented in a simplified manner which is based on microscopic considerations and leads to the macroscopically observed active behavior. One of the first such "mesoscopic" models was introduced by Nakazawa and Sekimoto who used continuum mean field kinetic equations to describe the one-dimensional dynamics of filaments moving relatively to each other due to the presence of cross-linking two-headed myosin motors [19, 20]. A closely-related approach was used by Kruse and Jülicher who found that the interactions of parallel filaments can lead to instability and contraction of bundles [21, 22]. Liverpool and Marchetti [23, 24] have generalized this approach to higher dimensions and studied the phase diagram of both homogeneous and inhomogeneous filament distributions,

taking excluded volume effects into account. More recently, a new phenomenological approach was proposed, treating filaments-motors systems as a viscoelastic polar active gel [25, 26]. In these generalized hydrodynamic theories, the dynamics is inferred from symmetry considerations [27, 28, 29, 30, 31] or by coarse-graining the mesoscopic kinetic equations [32, 33, 34]. Several inhomogeneous structures have been identified as steady-state solutions of the macroscopic equations, including asters, vortices and spirals. The same structures have also been predicted by Lee and Kardar [35], who used a somewhat different approach to derive two coupled dynamical equations for the filaments orientation field and the motors density. They also predicted the existence of arrested coarsening, a state in which areas in the system contain actin filaments devoid of motors. The model was later extended by Sankararaman *et al.* [36] to include populations of bound and free motors, as well as an additional coupling of filament orientation to motor gradients.

Simple phenomenological descriptions usually suffer from severe limitations when applied to complex systems involving many interacting participants. Molecular Dynamics (MD) molecular simulations can cope more effectively with the wealth of phenomena exhibited by such systems. For most biological systems the major problem with molecular simulations is related to the enormous computational cost required for a fully atomistic description of the system, which makes such simulations limited to very small length- and time-scales. For large-scale simulations, the system must be coarse grained to allow the emergence of results in a reasonable amount of time. Successful CG models use simplified representations of the participating molecules and the interactions between them, but they retain the fundamental physics which is responsible for the observed phenomena. (The process of designing such a model serves as an excellent "exercise" for identifying the basic physics of the system in question.) CG models have been applied to many biological systems, including biological membranes, trans-membrane proteins, and other biological complexes [37, 38, 39, 40, 41, 42]. They have been less frequently used for studies of self-organization of cytoskeletal filaments by molecular models. Nedelec and co-workers used this approach to investigate the dynamics in systems consisting of MTs and kinesin-like motors. In those simulations the MTs were represented as inextensible elastic polar rods and motors were modeled as small mechanical machines that walk over the MTs, bind them to each other, and lead to their relative movement. Using this model they managed to reproduce asters and vortices [43], study aster formation dynamics [44] and examine the effects of changing the probability of motor disconnection from the end of a filament [14]

In this paper we present extensive MD CG simulations of systems consisting of actin filaments and myosin II molecular motors. We study the self-organization behavior of the system and explore its steady state morphologies, as well as the dynamical evolution that leads to the formation of these structures. Generally speaking, the dynamics of the system is rather noisy, which can be attributed to the non-processive nature of myosin II motors which constantly bind to and unbind from actin filaments. Our simulations show how the motors are involved in the association, binding, and relative sliding of filaments which may lead to the formation of thick bundles. Another commonly observed steady state structure is asters, which over the course of time may fuse with each other to form bigger asters. Many of these asters tend to have four orthogonal arms (each of which may consist of many filaments) - a feature also observed in several experimental studies. Asters of long actin filaments may be connected to each other to form a mesh which eventually collapses. Our results, which agree well with existing experimental data, illustrate the richness of the phase diagram of myosin II-actin systems and reveal the role played by the multi-headed myosin II motors as active linkers.

The thesis is organized as follows: In chapter II we present the methods used to build the simulation emphasizing the biophysical model, computational design and the values assigned to important parameters. Chapter III deals with our results, demonstrating different types of bundles found, interesting aster features, and insights into the influence of the motor-filament ratio on the resulting structures. The last chapter summarizes important results, discusses some possible hypotheses and presents possible future work.

Chapter 2

Materials and Methods

This chapter is organized as follows: first, the biophysical model of the actin-myosin system is presented. It provides a layout of the physical equations that depict the essence of the system while maintaining computational feasibility. The second section presents the implementation of this model, introducing the problems we had to deal with and their solutions in our simulation. This section also introduces our graphical tool for displaying and analyzing the data. Last is a section presenting the parameters, explaining the considerations behind their assigned values.

2.1 The Biophysical Model

We aim at the simulation of a molecular system that includes water, actin filaments, aggregates of myosin II motors, the static linker protein fascin, an excess of ATP, and ADP [9, 5, 15]. The spatial and temporal scales of the phenomena that we simulate are on the orders of micrometers and minutes, respectively. On the other hand these phenomena arise from ATP hydrolysis, which take place on the nanometer and picosecond scales. Thus, the system is far too large and complex to be studied at the full microscopic level. It needs to be drastically simplified by hiding much of its complexity while still keeping its most essential characteristics. In this section we provide a formal description of our model along with an informal description of the decisions we made regarding the representation of the system.

The first major decision we made was to explicitly represent only two components of the system, namely actin and myosin. The other components will be considered only implicitly by their effect on the system's behavior. The presence of solvent is implicated by allowing non-bound myosin motors to diffuse and by over-damping force-driven movements. ATP hydrolysis is represented by the ability of myosin motors to move along filaments which

they are connected to. The presence of fascin is represented by rendering the actin filaments as stiff as bundles of fascin linked filaments. Thus, the second major decision was to represent static, fascin linked, bundles of actin filaments as single units. Along this manuscript we regard them as "filaments" to avoid confusion with the dynamic, ATP-hydrolysis driven, bundles whose formation is an emergent characteristic of our system. Single biological filament (which are the constituents of the "filaments") will be referred to as F-actin. Similarly, aggregates of myosin motors are represented as single motor units, with the number of motor heads and the total length of the motor aggregate defined by parameters. Finally, we have decided to simulate the actin-myosin system as pseudo two dimensional, which implies that our model does not include any excluded volume effect. This way, the common situation of two filaments lying one on top of the other is represented by two crossing filaments that do not interact.

Actin filaments are represented by linear chains of nodes. Each pair of neighboring nodes represent a segment of the filament with predefined length $l_{f,0}$. Thus the length of a filament is determined by its number of segments, with small variations due to the forces exerted on it which slightly change the lengths of the segments. The filaments are polar having plus and minus ends (see fig. 2.1(a)). The geometry and elastic properties of the filaments are governed by two energy terms: The first applies a Hookean spring [45] between each pair of neighboring nodes, keeping their mutual distance close to the predefined rest distance.

$$E_1 = \frac{1}{2}k_f(x_{i+1} - x_i - l_{f,0})^2 \tag{2.1}$$

where k_f is the filaments spring constant and x_i is the coordinate of the ith node (the vector notation is omitted for brevity). The second energy term, which represents the bending rigidity of the filament, assign the following energy term with each node (except for the two edges nodes) [2]

$$E_2 = \frac{1}{2}A(2x_i - x_{i+1} - x_{i-1})^2, \tag{2.2}$$

where A is related to the filament's persistence length, ξ, by $A = (\xi k_B T)/[2(l_{f,0})^3]$, where T is the temperature and k_B is Boltzmann's constant. The total energy of the filament is the sum of the above two terms for all the segments and nodes, and the associated force acting on the ith node is calculated by $f_i = -\partial E/\partial x_i$.

In our model actin filaments do not interact directly. The only way a filament may affect another one is through forces applied on them by motors that are bound to both

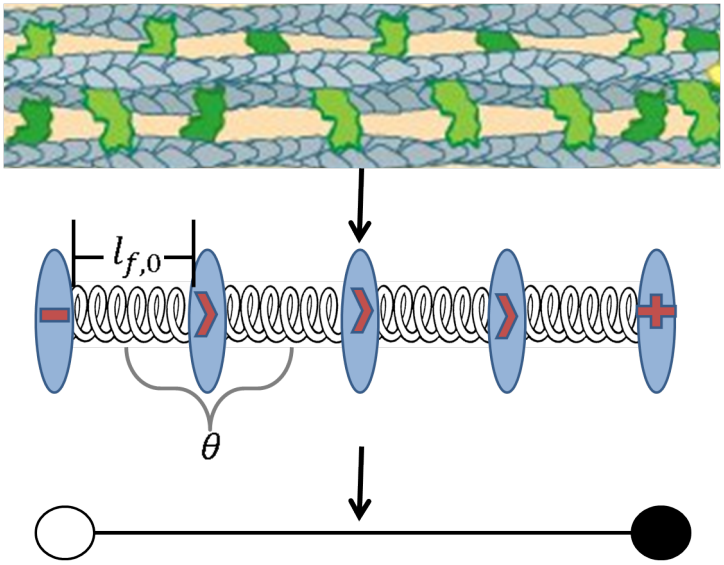

(a) Levels of abstraction of a F-actin

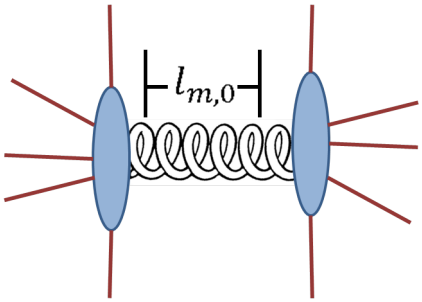

(b) Motor illustration

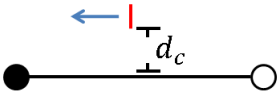

(c) Abstract representation of motors and filaments

Figure 2.1: Elements of the simulation. Figure (a) illustrates the process of abstracting the representation of a filament in our system. The first stage is a biological system, with G-actin bound to each other to give F-actin, and fascin binding the F-actin into bundles. The second stage shows the filaments represented by our simulation, which do not explicitly contain fascin, G-actin or F-actin. The filament is represented by an array of nodes connected by springs. These filaments are polar, having a plus end, marked by a plus sign, and a minus end, marked by a minus sign. The rest length of each of the springs is $l_{f,0}$ where f stands for filament. Filaments with no bending moment applied are straight. The third stage is that shown when visualizing the simulations results. It is a long rod, with a minus (empty black circle) and a plus (full black circle) end.

Figure (b) shows our motors. Each motor is defined by two nodes connected by a spring. Motors have many heads, with nodes having n_h heads each, all able to connect to a filament and progress along it.

In figure (c) we present a more abstract way of depicting motors and filaments. The motor is a short red rod. The filament is a long black rod with two ends. We denote the plus end with a full black circle, and the minus end with an empty black circle. This figure illustrates the proportions of a motor and a filament, with filaments being substantially longer than motors. The blue arrow marks the motors direction of progress, which is always towards the plus end. d_c marks the maximum distance from which a motor can connect to a filament with one of its heads. *Note that the distance d_c isn't in proportion to the rest of the figure.*

of them either directly or indirectly. Further, due to their large size the filaments do not diffuse significantly in the relevant time scales and, thus, the simulations do not include any treatment of their diffusion.

Motors are meant to represent a biological motor aggregate which is a long rod with an area at its middle with no heads, and with heads originating from all the rest of the aggregate. Our simulated motors have two nodes from which motor heads originate and a Hookean spring between them, with a length of $l_{m,0}$, with no heads emanating from it, to encompass these details. The energy of this spring is calculated in a manner similar to that used when defining a segment of a filament.

$$E = \frac{1}{2}k_m(x_{i+1} - x_i - l_{m,0})^2 \tag{2.3}$$

Where k_m is the motors spring constant. Every motor node has n_h motor heads originating from it (fig. 2.1(b)). Each of these heads is represented as a Gaussian spring (similar to a Hookean spring but with no rest length) with a node at its end, which is able to connect to a single actin filament. The energy of the motor heads spring is calculated in the same way as the spring between the two motor nodes (see eq. (2.3)), only with a different spring constant k_h and with no rest length (simplifies motion calculations of motor nodes not connected to filaments). As an aggregate is cylinder shaped, there are heads at 180^0 to each other which are therefore unable to connect to the same filament. We included this feature by specifying a maximum number of heads with which a motor can connect to a filament, denoted as max_h.

Once connected, a motor head starts advancing towards the filaments plus end. This motion is the main dynamical feature in the system, moving filaments relative to each other. A motor head has a characteristic speed v_0, which is the speed at which a motor progresses along a filament while no external forces are applied on it. The projection along the filaments axis, f_{axis}, of forces applied on a motor head, causes its velocity v to change as shown in fig. 2.2 and defined in the following equation [46]

$$v = \begin{cases} 2v_0 & f_{axis} \leq -f_0 \\ v_0 \cdot (1 - \frac{f_{axis}}{f_0}) & -f_0 \geq f_{axis} \leq f_0 \\ 0 & f_{axis} \geq f_0 \end{cases} \tag{2.4}$$

Note that due to the viscosity of the solvent, the forces do not cause the motors to accelerate.

Compatibility with the simulated biological system dictates that velocity may not exceed $2V_0$ and cannot be negative, that is the motors may stall but they never move backwards [46].

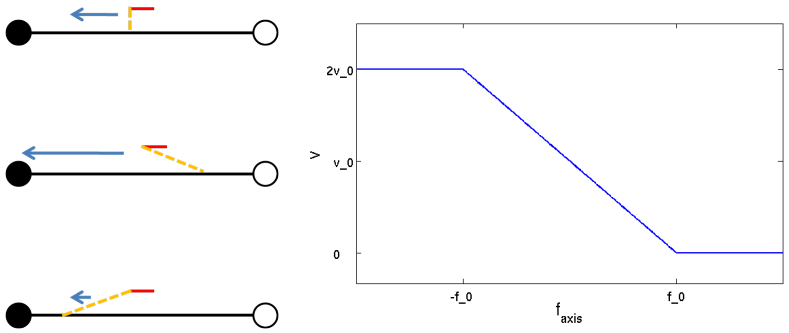

(a) Different scenarios leading to changes in the motor heads speed

(b) Motor head speed vs force

Figure 2.2: Figures illustrating the effect of force on the motor heads speed, as defined in equation (2.4). Figure (a) shows three different scenarios of a motor traveling along a filament. In these diagrams the length of the arrow shows the speed at which the motor head is proceeding towards the plus end (full black circle). In the uppermost schema the spring connecting the motor to the filament feels no force and progresses at speed v_0. The middle schema presents a case in which the spring is pulling the motor head forward increasing its speed. A motor head being slowed down is shown in the bottommost diagram.

The graph in figure (b) shows the speed of a motor head as a function of the force applied. The function appears as equation (2.4). As can be seen there is a maximum speed of $2v_0$ if the force pulling the motor head forward is equals to or greater than $-f_0$. If the force opposes the progress of the motor head, its speed declines until stalling when the force equals or exceeds f_0.

Motors cause the motion of filaments by transferring the force $F_{motor-head}$ applied on motor heads onto the two filament nodes on either side of the heads F_i ($i = 1,2$ denotes the first or second filament node). The force felt by each filament node is proportional to its distance l_i from the motor head as follows: $F_i = F_{motor-head}\left|\frac{l_f - l_i}{l_f}\right|$ where l_f is the current length of the segment between the two nodes. This equation implies that the node more distant from the head will feel less force (see fig. 2.3).

Motors can be found in one of two states - connected to or disconnected from filaments. If the distance between a motor and a filament is less than d_c (see fig. 2.1(c)) it has p_{con} probability of connecting in each simulation step. Once a motor has connected to a filament, it has a probability of p_{dis} to disconnect. The disconnecting probability, which depends on

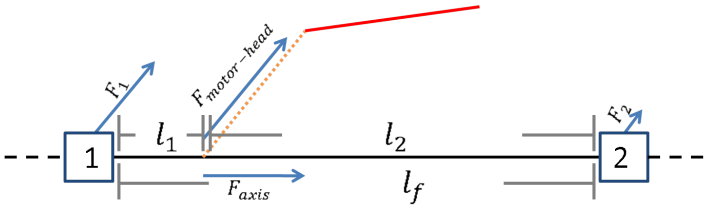

Figure 2.3: A force applied on a filament by a motor head. The red line denotes the motor, and the dashed orange line is the spring connecting the motor to the filament. The black rod is a segment with a filament node on each side depicted as blue squares. The distance of the motor head from each node is denoted l_i and the length of the segment between the two nodes is l_f. The forces applied are marked by arrows, with the forces size proportional to the arrows size. The closer the node to the motor head, the larger the portion of the total force exerted on this node. The projection of $f_{motor-head}$ on the filaments axis f_{axis} (which determines the motor's velocity of propagation), is also shown.

the force f exerted on the motor, is given by (see fig. 2.4)

$$p_{dis} = \begin{cases} 1 & f > \sqrt{f_{dis}^2 - 2k_h K_B T \ln(p_{min-dis})} \\ p_{min-dis} \cdot Exp\left(\frac{f^2 - f_{dis}^2}{2k_h K_B T}\right) & f_{dis} < f \leq \sqrt{f_{dis}^2 - 2k_h K_B T \ln(p_{min-dis})} \\ p_{min-dis} & f \leq f_{dis} \end{cases} \tag{2.5}$$

where $p_{min-dis}$ is the minimum disconnection probability possible in our system. This probability is applied when only a small force is felt by the motor head.

Our system is over damped [11], meaning there is no acceleration in the system. Therefore the speed at which nodes move is proportional to the instantaneous force they feel:

$$v_i = \frac{F_i}{\gamma}, \tag{2.6}$$

where γ is the drag coefficient of the node (either filament or motor node). The drag coefficient is different for motor nodes and filament nodes (see table 2.2).

Finally, the size of the step taken by each node is determined by their velocity as follows:

$$\Delta x_i = v_i \cdot \Delta t \tag{2.7}$$

Where Δt is the size of the time step in our simulation. For motor heads a diffusion factor

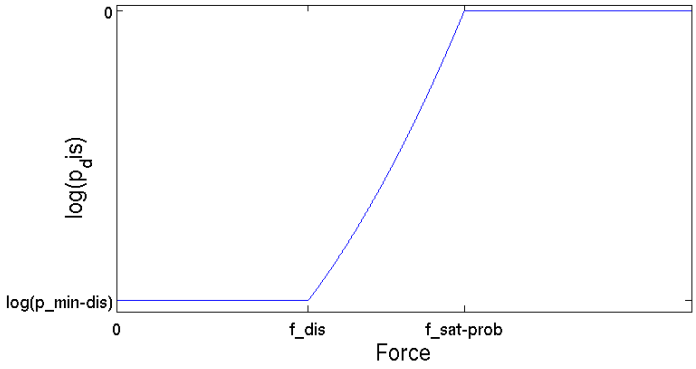

Figure 2.4: Graph showing the change in the log of disconnection probability vs the force applied on the motor head. This is a graphical representation of equation (2.5), and it shows the growth in p_{dis} once the force exceeds f_{dis}, until a force is reached $f_{sat-prob}$ at which the probability saturates.

has to be added which is determined by the following equation [11]:

$$\Delta x_i^2 = \frac{2K_BT\Delta t}{\gamma_m} \cdot rand \tag{2.8}$$

Where γ_m is the motor nodes drag coefficient and *rand* is a random number chosen from a normal Gaussian distribution. The first part of the equation $\frac{2K_BT\Delta t}{\gamma_m}$ is the standard deviation from the average displacement (which is 0) of a diffusing particle after Δt time. The random Gaussian element means that the particles motion isn't deterministic in nature, rather each time step it will diffuse a random distance.

2.2 Simulation Implementation

We coded our simulation in Java, as this language allows for fast development and can be debugged relatively easily. One of Java's advantages is that it is an object oriented language, making it possible to split the code into logical parts, i.e. motors and filaments. It also has powerful editors, debugging tools and performance analysis tools.

The simulation is based on a molecular dynamics model, which splits the overall simulated time into small time-steps Δt. Each Δt the forces felt by each motor and filament node are calculated and then the particles are moved to new positions according to these forces. Each iteration our system executes the following steps:

1. Check distances between filaments and motors to see if they can connect (whether $d < d_c$).

2. Check if motors connects to filaments or disconnect from them.

3. Calculate forces between each two nodes connected by a spring.

4. Calculate speed of motor heads connected to filaments.

5. Calculate movement caused by diffusion.

6. Calculate new coordinates, based on previous calculations of forces, motor heads speeds, and diffusion.

The boundaries of the simulation are periodic, meaning that filaments reaching the edges of the simulated area, reappear on the other side. This choice of boundary conditions reduces finite size effects which are negligible in experimentally large systems. These boundaries can be described by using the following equation: $nc \leftarrow cc \bmod sd$. sd is the size of the simulation in one of the dimensions, cc is the calculated coordinate and nc is the new coordinate. This equation promises that: $nc < sd$. We preferred a more computationally efficient equation:: $nc \leftarrow cc - sd$, which can be used if cc is never greater than $2 \cdot sd$. This is true if we assume that the step size of nodes is much smaller than sd. Not only coordinates need to be dealt with in a periodic system, but also lines connecting two coordinates demand special treatment. One point worth noting is the calculation of distances between two nodes. Let us assume a one dimensional periodic system in which one of the nodes has a coordinate of $sd-1$ and the second has a coordinate of 1 ($sd >> 1$). Without periodic boundaries the distance is simply $dist = (sd-1)-1 = sd-2$. In a periodic environment, this is not the case as the second node's coordinate may also be seen as $sd+1$, therefore the distance between them can also be 2 as illustrated in figure 2.5. Our system solved this problem by choosing the smaller of the two distances.

Our simulation is pseudo two-dimensional, meaning that although we use only two axes, we didn't implement excluded volume, allowing filaments and motors to overlap as if there is a third axis. This was done as overlapping of filaments is part of the dynamics necessary for self-organization. This has it drawbacks, as we can't simulate motor traffic jams, which may have interesting effects. A problem we encountered as we didn't implement excluded volume was large numbers of motors aggregating at the center of our asters (see Introduction), many more than physically possible, which meant there were great forces at the asters center and that most of the simulation was devoid of motors. One work around we found was to place an upper limit on the number of motor heads able to connect to a filaments plus end, denoted as max_{fp}. We limited only the number of motor heads connecting to a plus

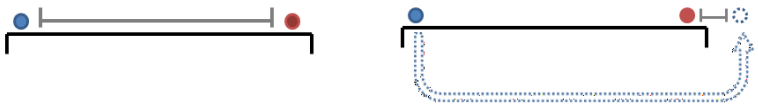

(a) Distance without periodic boundaries (b) Distance with periodic boudaries

Figure 2.5: Comparison of distance calculation with and without periodic boundaries, in a one dimensional system. Figure (a) shows the distance between two points in a system without periodic boundaries. Fig (b) shows the distance between the same two points in a periodic system. The distance between the two points, can be measured with the blue circle shifted, as shown by the dashed arrow, to a position much closer to the red circle, as like on the surface of a ball there are two paths between two points. Therefore there is a shorter distance between them than in the system depicted in fig. (a).

end as nearly all motors aggregate there. A motor head which connects to a filaments plus end after the limit has been reached, is immediately disconnected, as are all other bound motor heads originating from the same motor, and the motor as a whole is repositioned at a new random coordinate. Merely disconnecting it without relocation doesn't solve the problem, as asters centers are dense with filaments, meaning the motor will stay in its immediate vicinity and will not manage to diffuse outwards.

Every iteration it is necessary to find the filaments close enough to each of the motors for a connection to be established. The simplest solution is to calculate the distance between every motor and filament to see if they are close enough. This process is time consuming, especially as it is done every time-step. We therefore chose to solve the problem by implementing a grid. A grid splits the simulated area into cells each of which registers all particles in it. When a motor searches for neighboring filaments, it needs to check only those in its 9 neighboring cells. This solution works well if excluded volume is enforced, as the number of particles in the cells is limited. As motors and filaments tend to accumulate and as our system doesn't implement excluded volume, the number of particles in some of the cells grows as the simulation proceeds, causing a slow down. We found our system slowed down by a factor of 2-3 as the simulations proceeded.

Regarding motors diffusion, we noticed that many motors diffuse locally in areas empty of filaments, resulting in many staying unbound, and wasting dear computational time. This may be a more exact biological description, but wastes a precious resource. We therefore decided to change the rate of a motors diffusion as a function of its distance from the nearest

filament. The greater the distance, the faster the diffusion. This causes all motors to be drawn towards the filaments, bringing the number of "idle" motors wasting our resources to zero. As we have a grid, motors may not know the distance to the closest filament, if there are no filaments in the 9 cells it searches in. This means there is a maximum radius in which a motor searches, which we denoted as max_{dist} (see fig 2.8(b)). For motors with a distance of at least max_{dist} from the nearest filament, we placed an upper limit on diffusion speed, denoted as max_{diff}. Motors close enough to connect to a filament do not receive a boost. The equation describing the accelerated diffusion is as follows:

$$\Delta x_{cm} = max_{diff} \times f(dist) \times rand \tag{2.9}$$

$$f(dist) = \begin{cases} 1 & dist > max_{dist} \\ \frac{dist - d_c}{max_{dist} - d_c} & d_c < dist < max_{dist} \\ 0 & dist < d_c \end{cases}$$

Δx_{cm} is the motors center of mass, implying that each of the motors two nodes will move this amount (Δx_{cm}) because of accelerated diffusion. $f(dist)$ is a function which receives the distance of the motor from the closest bundle and returns a value between 0-1 depending on how close the motor is to the bundle. The closer the motor to the bundle the smaller the value of $f(dist)$. *rand* is a Gaussian random generator. Equation (2.9) is illustrated in fig. 2.6.

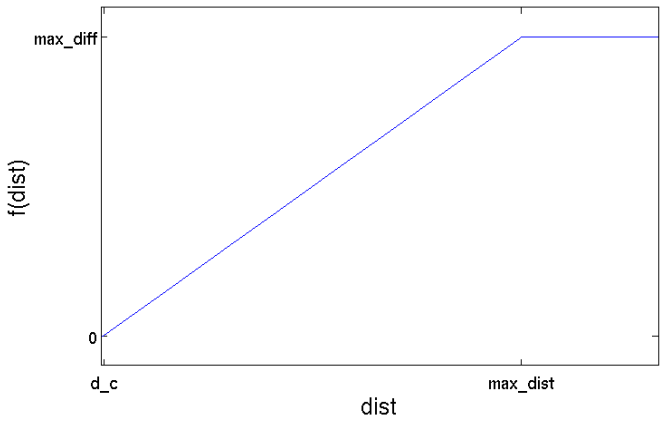

Figure 2.6: Graph of boosted diffusion showing the size of the maximum diffusion step as a function of the distance of the closest filament to a motor. The size of the actual step also depends on the random number generator as shown in eq. (2.9).

Much data is created by our system, as each iteration the forces and coordinates of each

node of a filament and motor are calculated as well as the position of the motor heads. We chose to save the data in its raw form, i.e. we save the coordinates of all motor and filament nodes. Not all of this data is saved, our simulation creates a file with the coordinates of all motors and filaments only once every $\Delta frame$ iterations. This is done as saving all information would demand much storage space, and in addition it is not necessary to save all iterations to capture the dynamics. Moreover, it is sometimes easier to understand the dynamics as a whole by omitting some of the fine details. We represent the data in a graphical form as shown in fig. 2.7. Filaments are represented as long black rods and motors as short red rods. The connection of motors to filaments isn't shown as it is too short and can't be seen. Our graphical tool reads the all the files of a simulation sequentially, showing a film of the simulations results.

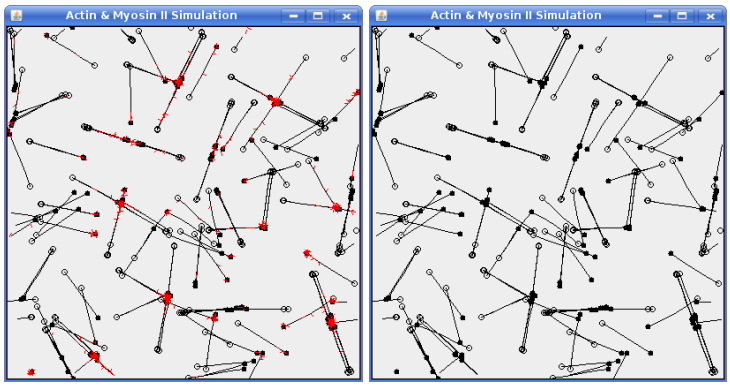

(a) Example of full system (b) Only filaments being shown

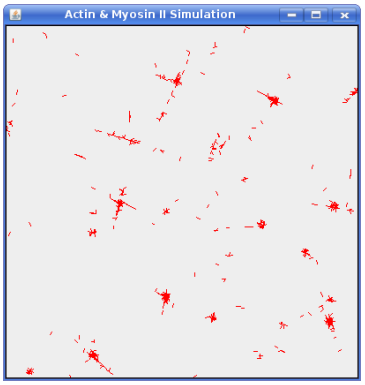

(c) Only motors being shown

Figure 2.7: Example showing the graphical representation of our simulation. Fig. (a) shows all the visualized features. The filaments are long black rods with their plus end marked by a full black circle and their tail marked by an empty black circle. Motors are shown as red rods. The other two figures illustrate some of the options available for easier analysis. Fig. (b) shows the option of exhibiting only the filaments participating, while fig. (c) shows the same instance of the simulation exactly, with only the motors visible.

2.3 Parameters

The spring constant k between adjacent notes of the actin filaments is dictated by the following stability criterion relating k, to the drag coefficient γ and the simulations step time Δt:

$$\frac{k}{\gamma} \times \Delta t < 1 \tag{2.10}$$

If this criterion is disobeyed then the length of the actin segment grows without bound (rather than being restricted to small variations around the rest length). If the spring constant is large either the time-step needs to shrink, which causes an increase in execution time, or the drag coefficient needs to grow, which isn't a good solution either as it slows the simulation down. This criterion holds for motors and filaments.

Regarding the spring constant of a filament segment k_f, there was another important factor deciding its value. Each filament segment represents $800nm$ of the total filament, which is much longer than a single G-actin. Therefore there is variance in the distance between the two ends of the segment as the G-actin it represents do not necessarily align along a straight line due to thermal noise. This effect can be simulated by the springs constant, defined as follows [11]:

$$\langle R^2 \rangle = 2\xi^2 \left[exp(-\frac{L}{\xi}) - 1 + \frac{L}{\xi} \right] \tag{2.11}$$

This equation gives the average length R given L the max length, where ξ is the persistence length. Using this equation an F-actin with a maximum length (L) of $810nm$ will have an average length R of 800nm. In our system this can be modeled well by a spring with a rest length of $800nm$ and a spring constant of $0.05\frac{pN}{nm}$. This allowed us to assign a segments drag coefficient, $\gamma_{F-actin}$, a value of $9.6e-7\frac{pN \cdot sec}{nm}$ and the time step, Δt a value of $10^{-7} sec$.

Simulated filaments containing more than one F-actin have different physical properties determined by the number of F-actin in the filament. For example the drag coefficient γ_f grows as a function of the number of F-actin, n_f, as follows: $\gamma_f = \gamma_{F-actin} \times n_f^{1/2}$. The reason for the power of $1/2$, is that the surface area grows as a power of two of the radius of a single F-actin, and the drag coefficient is a function of the radius as given by Stokes law $\gamma = 6\pi\eta r$[11]. Another parameter which varies with the number of F-actin is the persistence length ξ, which scales as r^4 where r is the radius of the filament, therefore it scales as n_f^2, as the cross section scales as $\sqrt{(}r)$, leading to $\xi = \xi_{F-actin} \times n_f^2$. [47].

One of the decisions which needs to be made is the size of the grid cells. On the one

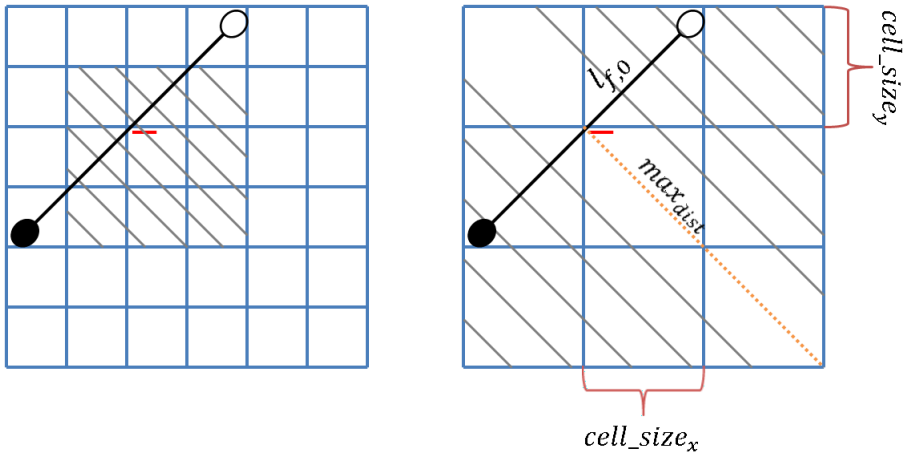

(a) Bad choice of grid cell size

(b) Correct size of grid cell size

Figure 2.8: Illustration of the lower bound of the cell size. In both figures the cell is depicted by a blue grid. The cells the motor checks to see if there are any neighboring filaments are marked by grey diagonal lines. Fig. (a) shows a case where a motor is close enough to a filament for a connection to be made, but the filaments plus and minus ends are not in the cells neighboring the motor, therefore the motor will not know of the filament and will not connect to it. Fig. (b) shows the solution to this problem. The size of a cell needs to be close to half the length of $l_{f,0}$. This promises that even in the worst case (depicted in the figures), the motor will always know of nearby filaments.

Fig. (b) also shows the meaning of max_{dist}, i.e. the maximum distance at which a motor checks if there are any neighboring filaments. This distance is the diagonal crossing two cells (the orange dashed line).

hand the bigger the cell, the more particles there will be in each cell reducing its efficiency. On the other hand, cells which are too small will waste a lot of computational memory for maintaining all of the cells. Therefore, in most cases, the size is chosen so that most cells will be populated by one or two particles. In our case there was another consideration which had to be taken into account and that was the distance between two neighboring filament nodes $l_{f,0}$. Let us suppose we choose a small cell size (see fig. 2.8(a)). It is possible the filament is very close to a motor but the nodes defining this segment are not in any of the cells surrounding the motor. Written in a mathematical form, the constraint is as derived from Pythagoras's' theorem: $\sqrt{2 \cdot cell\_size^2} > l_{f,0}/2$ (see fig. 2.8(b)). This leads to cell size of $283nm$. To promise that we had a whole number of cells and that we didn't have too many cells we chose the size of the cell to be $400nm$.

We simulated systems under different concentrations of G-actin and myosin II. All simulations were initiated with filaments and motors randomly distributed in the system. We executed each of the different experiments 5 times, each with a different random initial layout of the filaments and motors. Our time step was $\Delta t = 10^{-7} sec$ and we ran the simulation for 16 seconds (unless explicitly mentioned otherwise all times are simulation time and not real time). We studied the temporal evolution of the system, analyzing the dynamics of the experiment as it progressed in time.

A technical problem we encountered was that our simulations take a long time to execute (a few months) and on this scale of time, computers tend to crash/shutdown etc. We dealt with this, by implementing a backup system. Our simulation writes a backup file, every $\Delta backup$ iterations. The number of iterations cannot be too small, for then the backup system will take too much time. If we make it too big, we will loose much information on a computer crash.

We simulate systems containing either a total number of 960 or 1920 actin segments. The number of segments per filament and the number of motors vary where, in general, the number of motors per filament will be smaller for shorter filaments and greater for longer filaments. The data is summarized in Table 2.1.

(a) **Experiment 1**, 960 segments in each experiment

number of segments per filament	4	8	12
5 motors per filament	240,1200	—	—
∼10 motors per filament	240,2400	120,1000	80,800
∼20 motors per filament	—	120,2000	80,1600

(b) **Experiment 2**, 1920 segments in each experiment

number of segments per filament	4	8	12
5 motors per filament	480,2400	—	—
∼10 motors per filament	480,3600	240,2000	160,1600
∼20 motors per filament	—	240,3000	160,2400

Table 2.1: Data for both sets of simulations. Columns show the number of segments per filament (also implicating a different number of filaments in the system, as the total number of segments is constant). Rows represent the number of motors per filament. The values in each box are the total number of filaments in the system and the total number of motors in the system respectively.

Table 2.2 summarizes all parameters, there meaning, there values and an explanation or citation as to why this is there value.

Name	Description	Value	Explanation
General Parameters			
sd_x	Simulation dimensions, x axis	$20000nm$	1
sd_y	Simulation dimensions, y axis	$20000nm$	1
$cell\_size_x$	Size of grid cell, x axis	$400nm$	function of $l_{f,0}$
$cell\_size_y$	Size of grid cell, y axis	$400nm$	function of $l_{f,0}$
$\Delta backup$	Number of iterations between two backups	20000	2
$\Delta frame$	The number of iterations between two frames saved	200000	3
Δt	The time difference between two iterations.	$1E-7sec$	stability
Filament Parameters			
k_f	Filament spring constant	$0.05\frac{pN}{nm}$	stability
$\gamma_{F-actin}$	F-actin drag coefficient	$6E-9\frac{pN \cdot sec}{nm}$	stability
$l_{f,0}$	Rest length of spring between two filament nodes	$800nm$	stability
n_f	The number of F-actin per simulated filament	3	4
$\xi_{F-actin}$	F-actin persistence length	$15000nm$	see [11]
dia_f	F-actin diameter	$19nm^2$	see [11]
dia_g	G-actin diameter	$5nm$	see [11]
max_{fp}	Max number of motor heads which can connect to a filament plus end	40	5
Motor Parameters			
k_m	Motor spring constant	$5\frac{pN}{nm}$	6
k_h	Motor Head spring constant	$0.25\frac{pN}{nm}$	7
γ_m	Drag coefficient of motor node	$5.5E-7\frac{pN \cdot sec}{nm}$	8
$l_{m,0}$	Rest length of spring between two motor nodes	$200nm$	9
$l_{h,0}$	Rest length of spring between motor node and motor head	0	10
n_h	Number of motor heads on each node	10	11
max_h	Maximum number of heads with which a motor can connect to a filament	4	11
d_c	Maximum distance at which a motor head can connect to a filament	$8nm$	7
v_0	Motor head speed on filament, with no external forces applied	$6000\frac{nm}{sec}$	see [11]
f_0	Force at which Motor head stalls	$2pN$	see [11]
$p_{min-dis}$	Minimum probability of motor head to disconnect from filament	0.5 after $5nm$	12
f_{dis}	Force at which probability to disconnect is $p_{min-dis}$	$10pN$	13
p_{con}	Probability of motor head to connect	0.0017	14
max_{diff}	Max distance a motor can diffuse if it is distant from all filaments	$100nm$	15
max_{dist}	Max distance a motor can measure to a filament	$1131nm$	function of cell size

Table 2.2: Summary of Parameters. All parameters in our simulation are mentioned, with a short description, their values and a reference as to why we chose this value. The reference may be a citation, a reason we elaborated on previously in the text or a number referring to a paragraph following this table.

1. The size of the simulation should be chosen so that on the one hand a filaments plus end will not meet its minus end, because the simulation box is too small and because of periodic boundaries. On the other hand, it shouldn't be too large, as this requires many motors and filaments to achieve a high concentration, which demands much computational time.

2. The number of iterations between backups shouldn't be to scarce as this misses the point of backups, while backups done too frequently cause the simulation to slow down.

3. The number of iterations between two frames saved should not be too small as it will slow the execution of the simulation. It can't be too big as much of the dynamics will be lost.

4. Choosing the number of F-actin per filament to be 3, means that short filaments are quite stiff, while long ones are quite flexible, allowing us to understand the dynamics of different stiffnesses without changing the thickness of the filament.

5. The maximum number of motor heads which can connect to a filament plus end was chosen to accommodate two factors. The first was to allow as many motors as possible to leave the filaments plus end emulating some form of excluded volume. The second was to maintain the structures already formed and prevent them from being pulled apart by other motors, by leaving enough motors connected at the filaments plus ends to oppose these destructive forces.

6. Our Motor spring constant was chosen to be greater than the spring constant between two filament nodes as it is shorter and as myosin II aggregates are thicker and stiffer than F-actin. Another consideration was the stretch caused by motor heads. The value chosen for the motors spring constant promises that the spring will not usually stretch more than 10% of its length (meaning a stretch of $20nm$), even if all motor heads are bound and applying force on the node.

7. We chose the motor head spring constant such that if it connected from the maximum possible distance the force it felt wouldn't be greater than f_0 (the stall force). The fact that the spring constant is relatively weak (considering the spring is rather short) also means that the motor head can proceed without constantly stalling. The maximum distance at which a motor head can connect is $8nm$, approximating the biological

value [18].

8. Motor nodes drag coefficient was assigned a value larger than that of filament nodes as motor nodes are physically larger. Another consideration was that the motors spring is stiffer, therefore a stable system demands either making Δt smaller or increasing the value of the drag coefficient.

9. We simulate 20 single myosins in each motor aggregate, which leads to the assignment of 10 motor heads per node. As the length of a single myosin II motor is $150nm$ [1], and taking into account the bald area of the aggregate, the length of each motor aggregate should be approximately $200nm$.

10. The rest length of the spring between a motor node and a motor head was chosen to be 0. This means that when unbound the motor head has no effect on the motors movement which simplifies the simulation.

11. The number of heads on each node emulates a medium sized aggregate. Limiting the number of motor heads which can connect to a single bundle has physical justification as mentioned above. It also allows a motor to interact with more surrounding filaments, giving rise to richer dynamics.

12. Myosin II moves forward with steps approximately $5nm$ in size [18]. To promise a fair chance the motor will manage to complete a step, we defined a probability of 0.5 that the motor stay connected for every 5nm it proceeds.

13. We chose the maximum force at which the probability to disconnect is 0.5 to be 10pN, to ensure that if stronger forces were generated the motor would immediately disconnect, so as not to cause large distortions of the spring. We didn't chose a smaller force, to enable motors to proceed without disconnecting immediately. Another reason is that during complex dynamic changes, quite large forces are generated, which would cause all motors to disconnect if the force was to low, leading to a loss of dynamic features in our system.

14. We would like to have a probability of 95% that a disconnected motor will be able to diffuse to a distance from which it cannot reconnect to a filament ($8nm$). The number of iterations it takes to diffuse 8nm can be found from the diffusion equation $< x^2 >= \frac{kT*2*\Delta t}{\gamma_m}$ therefore $\Delta t \approx 30$. This leads to the probability equation $(1-p)^{30} = 0.95$. The result is p=0.0017, which means that the probability to connect each iteration is

very small. This is related to non-processivity of the motors, as it means that single motors will not manage to proceed large distances along a filament, for once it has disconnected it will not usually be able to reconnect.

15. The maximum distance a motor can diffuse when distant from all filaments, is not too big, so as not to move motors out of their local area, while still big enough to allow them to bind to bundles out of their current reach.

Chapter 3

Results and Discussion

The analysis of a complex system can be done at different scales. In our system, at the smallest scale one can watch single motors and filaments. At a larger scale, it is possible to observe the interactions of a number of filaments and motors. At the largest scale, whole system dynamics and steady states can be studied. In this chapter we will examine the different features, from the bottom up. The smallest scale features are the stochastic behavior of our simulations and the relative motion of two filaments. Next we will discuss the creation of bundles and their different steady-states. After that, aster formation and stability will be considered, Finally we will show the influence of motor concentrations and filament lengths and concentrations on the dynamics and steady-states observed.

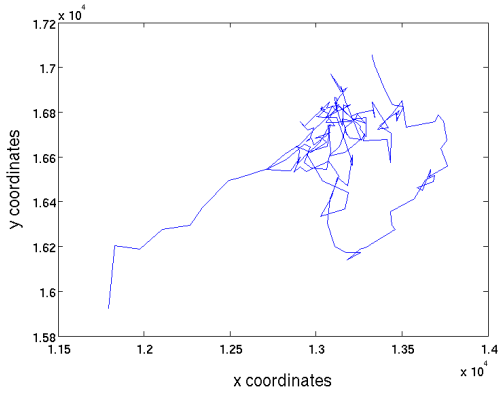

Figure 3.1: A graph following the movement of a single filament plus end, for the length of a simulation. The axes are x,y coordinates of the plus end. The line connecting the points shows the order of occurrence, with two points connected occurring sequentially. As can be seen the motion of a filament plus end is quite noisy, with changes in direction occurring continuously. Of course the motion is not entirely stochastic as motors move in a well defined direction.

The smallest scale feature of our dynamics is its noisy nature as shown in fig 3.1. This

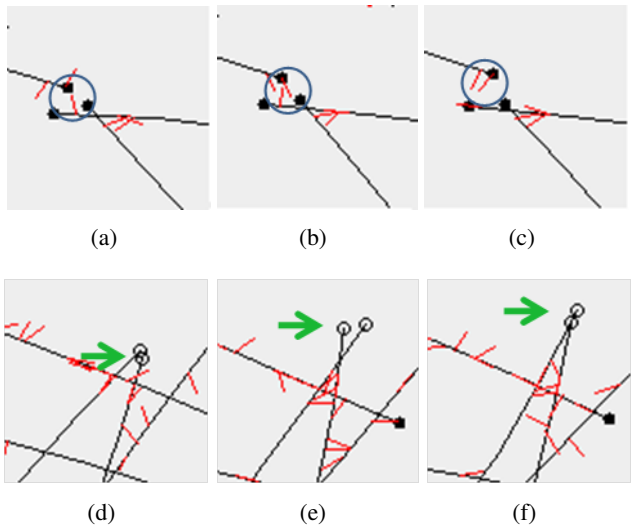

Figure 3.2: These figures show some of the stochastic dynamics of our simulation. The blue circle in (a)-(c) focuses on an area with three plus ends (full black circles) exhibiting the noisy nature of motors (short red rods) caused by their non-processivity. This area shows motors acting as linkers intermittently. At first (fig. (a)) only one motor connects the filaments in the area marked by the blue circle. In fig. (b) 2 motors are acting as linkers between filaments and in fig. (c) all motors have disconnected due to their non-processivity.

Figures (d)-(f) illustrate the noisy nature of the filaments movement, This movement is marked by a green arrow. The two filaments start off with their minus ends (black empty circles) overlapping (fig. (d)). Next the minus ends are separated (fig. (e)) and finally they overlap again (fig. (f)). If movement was continuous and smooth, the distance between the filaments minus ends should have increased or decreased continuously. This motion cannot be explained by diffusion as filaments do not diffuse in our model.

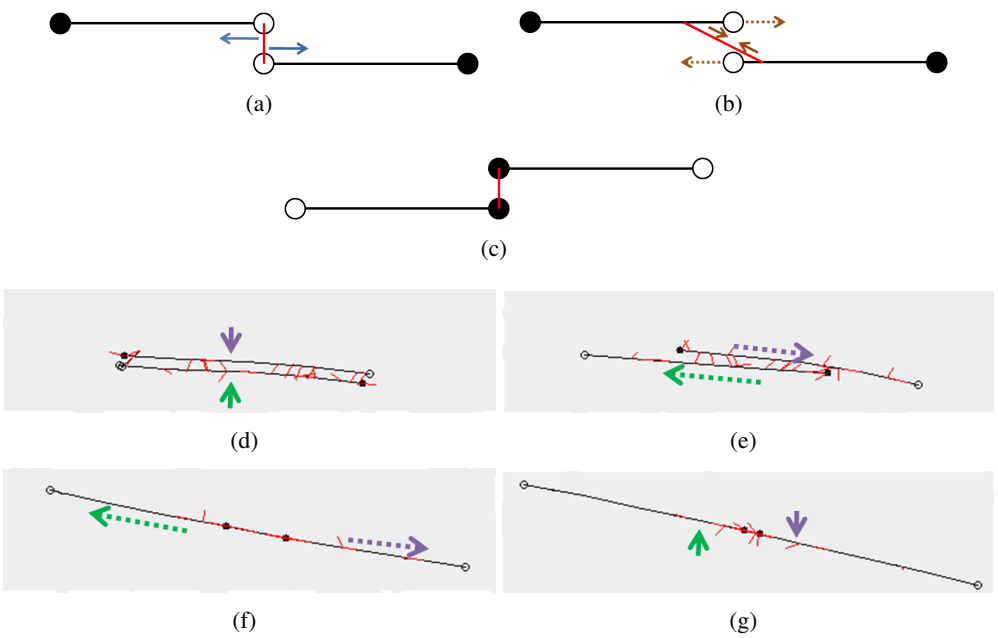

Figure 3.3: Relative motion of anti parallel filaments. Figs.(a)-(c) are a schema of anti parallel motion. In fig (a) two filaments (long black rods) are initially aligned minus end to minus end (empty black circles), with a motor between them (red rod) progressing towards both filaments plus ends (shown by blue arrows). This motion creates a force, shown by brown arrows in fig. (b), whose projection along the filaments axis (shown by dashed brown arrows), moves them until they finally reach a state in which the motors cannot proceed (fig. (c)).

The snapshots show the sliding caused by motors moving along two filaments simultaneously. The green and purple arrows points at the two filaments. As can be seen ,in figure (d), they are aligned in an anti-parallel fashion. Figures (e)-(f) show the direction of motion of both filaments with dashed arrows. Figure (g) shows a final steady state, in which the motors are connected to the plus ends of both filaments, and can progress no more.

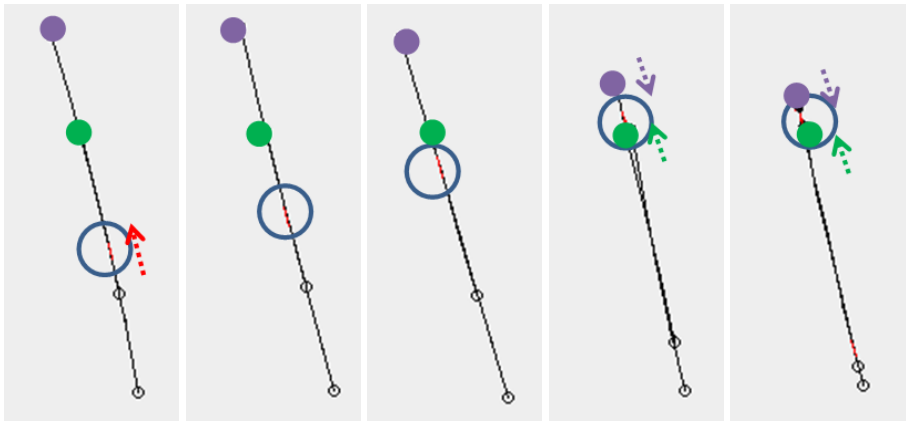

(a) (b) (c) (d) (e)

Figure 3.4: Relative motion of parallel filaments, with plus ends in the same direction. The blue circle marks a motor (short red rod) advancing towards the plus end (green and purple full circles) of two filaments. In figure (a) the motor can be seen, with a dashed red arrow pointing in its direction of progress. Figures (b)-(c) display the motor advancing without causing any relative movement between the filaments it is connected to (the distance between the two colored heads doesn't get any samller), as it is doesn't stretch, therefore applying no force on these filaments. Figures (d)-(e) show relative motion caused when the motor reaches the plus end (green full circle) of one of the filaments, ceases to move along it while continuing to progress along the second filament (purple full circle), stretching and creating a force which causes relative motion. The direction of motion of each of the colored heads is marked with a dashed arrow of matching color.

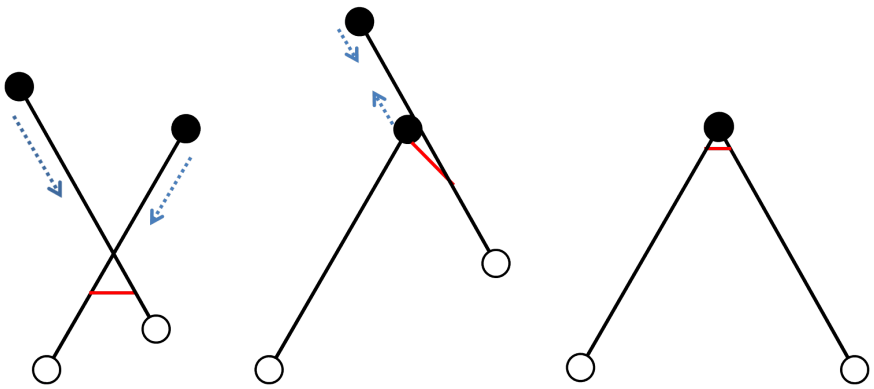

(a) X configuration (b) T configuration (c) V configuration

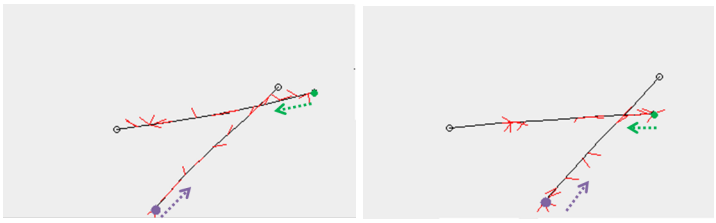

(d) X configuration (e) X configuration

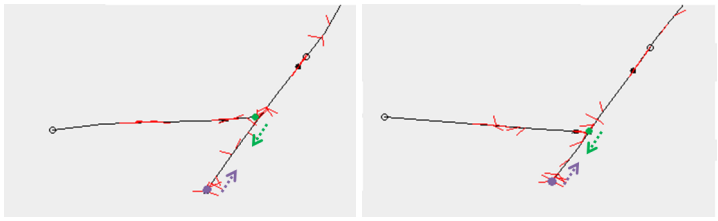

(f) T configuration (g) T configuration

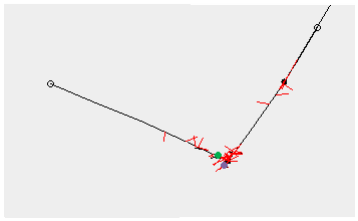

(h) V configuration

Figure 3.5: Relative motion of intersecting filaments. Figures (a)-(c) are a schema of the three configurations of overlapping filaments. Fig. (a) shows a X configuration with blue arrows showing the direction in which the motor progresses, pushing the filaments back until a T configuration is reached (fig. (b). At this point the motor progresses only along one of the filaments as shown by the blue arrow, until the motor reaches the plus end of both filaments which then resemble a V shape. At this stage the motor can proceed no longer and a steady-state has been reached.

Figures (d)-(h) show an example of these dynamics as seen in our simulations. The plus end of the filaments of interest are marked as purple and green full circles. The initial configuration of the two filaments is a X. In figures (d)-(f) the two filaments slide along each other. Each of the filaments is moving towards the other filaments plus end, with directions of movement marked by dashed arrows, each with its color matching a filament. In (f) the purple filament has reached the green filaments plus end and ceases progressing along it, transforming the X into a T shape. Afterwards the green filament continues along the purple filament until it in turn reaches the purple filaments plus end in figure (h) and now a V shape can be seen. At this point neither filament can progress.

feature is caused by many factors. The first reason is the influence of thermal agitation on motors. Another, is the non-processivity of our motors, which connect and disconnect stochastically. This means that filaments don't slide smoothly along each other, rather a motor bound to two filaments will cause a short burst of relative movement, after which it will disconnect, causing the filaments to disconnect (if it is the only motor connecting them) or the speed of movement to change (if other motors also connect these two filaments). Figures 3.2(a)-3.2(c) show the non-processivity of motors which connect and disconnect stochastically. The noisy influence of myosin II motors has already been studied *in-vitro*[48, 45], establishing them as a major source of random noise. This can be seen in figures 3.2(d)-3.2(f) which exhibit the noisy nature of the filaments movement, caused by motors. This stochastic behavior hasn't been mentioned in previous CG-MD simulations of the cytoskeleton, which is not surprising as most such simulations include kinesin motors which are highly processive.

Apart from creating a stochastic environment, our motors also reorganize the filaments layout by moving them relative to each other. The smallest scale of reorganization is between two filaments which can be aligned in three possible ways, each leading to different dynamics. The first is if the two filaments are anti-parallel, meaning that the plus ends of both filaments are pointing in opposite directions. In this case the motor moving along the filaments towards their plus ends, is moving in two opposite directions, it therefore stretches and creates a force pulling on both filaments. Figure 3.3 illustrates this feature, with figs. 3.3(a)-3.3(c) showing a schema of a motor and its effect on anti-parallel filaments, and figs. 3.3(d)-3.3(g) showing this feature as observed in our simulations. A second possible alignment is two filaments parallel to each other. A motor traveling along them will not usually cause the filaments to move as the motor does not stretch while progressing along them (fig. 3.4(a)-3.4(c)). This is the case as long as the motor hasn't reached the end of one of the filaments, while still progressing along the second one. In this scenario the motor ceases moving along the first filament while still progressing along the second one causing the motor to stretch and apply force on the filaments, giving rise to their reorganization (fig. 3.4(d)-3.4(e)) [19, 49, 50].

A third possibility is that the two filaments are not aligned along a common axis. A possible state is of the two filaments overlapping, creating a structure resembling an X. If the two intersecting filaments are connected by motors at only one point, the filaments will move towards each others plus end, as can be seen in figure 3.5. At first the configuration

will transform from an X to a T shape, when the motor reaches the plus end of one of the filaments. The final shape will be a V, after the motor reaches the plus end of the second filament. This form of self-organization seems to be the method leading to asters and has been mentioned previously by Nedelec[44]. If the filaments are connected at more than one point (for example on both sides of the X intersection point), rotational motion may be observed, resulting in the collapse of the X configuration into a one-dimensional structure as discussed later on in this chapter.

3.1 Bundles

Over longer periods of time our system is reorganized into several different patterns, the most basic and simplest of which being bundles. Bundling starts when neighboring filaments are connected by myosin motors which cause them to align parallel to each other and unite (see figure 3.6 for a possible scenario). Although the linkers in our system are always myosin motors which are not static, after reaching the plus ends of the filaments, the bundle created will stay stable, as the motors have reached a point from which they cannot advance.

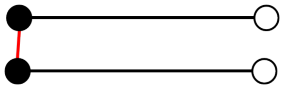

Figure 3.6: A schema of a thick bundle. The filaments are aligned side by side with the motors (short red rod) concentrated at their plus ends (full black circle).

Bundles linked by myosin can be found in three different forms in our system. The first type is *thick bundles*. These bundles aren't longer than a filament, but they are much thicker. The filaments are arranged alongside each other, with all filaments having the same polarity as can be seen in figure 3.7(d). The simplest dynamics leading to thick bundles is shown in figures 3.4(d)-3.4(e), where two parallelly aligned filaments are organized into a thick bundle. If the two filaments are in a V configuration, rotational motion is needed to create a thick bundle. Rotational motion demands at least two points at which motors link the two filaments as one of the points needs to serve as a rotation axis see 3.7(c). Filaments inherent stiffness is also important for rotation to occur. Without this stiffness, a force applied on the filament would only cause a local distortion, leaving the rest of the filament unaffected. This rotational motion doesn't seem to be caused by motors pulling the filaments togehter at just one point, rather there seems to be a steady flow of motors each connecting the two filaments at an additional point in a manner resembling the closing of a zipper.

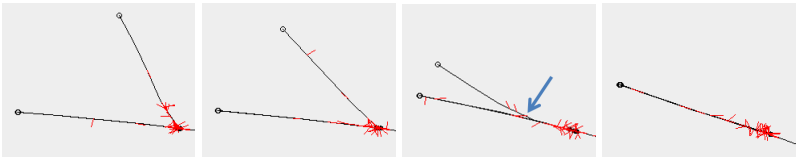

(a) (b) (c) (d)

Figure 3.7: An illustration of rotational movement leading to the creation of a thick bundle. Figure (a) shows the initial state in which two filaments are connected at one end but are not alongside each other. Figures (b)-(c) show the process of the two separate filaments uniting into one thick bundle which can be seen in fig. (d). Figure (c) is of special interest as it illustrates the dynamics leading to rotational motion. This figure depicts two filaments connected by motors at two points; the first is at the filaments plus ends which serves as an axis of rotation. The second is approximately a third of the way along the filaments and is marked by a blue arrow. The deviation of the upper filament from a straight line can also be seen, which also leads to the unison of the two filaments. These figures also seem to suggest that the closing of the filaments isn't attained by only two points of connection, rather there are many points of connection, caused by a continous flow of motors, each connecting the two filaments at an additional point, resembling the closing of a zipper. This steady flow of motors can be seen in figures (b)-(c) and can also be deduced from the growth of the number of motors at the filaments plus ends (marked as full black circles). Together these connections and the fact the filaments are stiff, meaning that a local distortion has a global effect, can cause rotational movement, aligning the two filaments relative to each other.

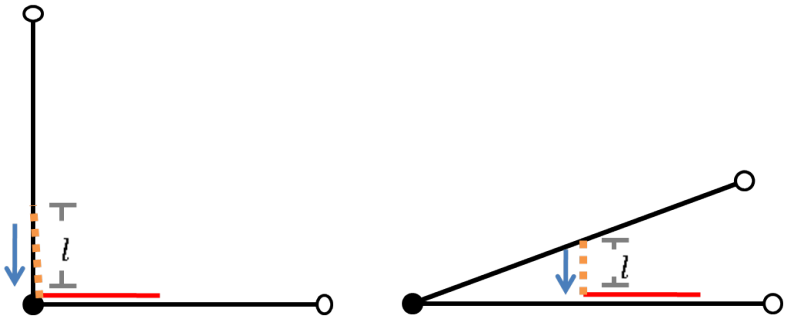

(a) (b)

Figure 3.8: The two schemas compare the ability of a motorhead to create rotational force, which will cause the two filaments to collapse into a thick bundle. Figure (a) shows two filaments with 90^0 between them. The motor (short red rod) is connected to both filaments, with the motorhead connected to the more distant one shown by an orange dashed line. Motor heads are modeled as a node connected to the bulk of the motor by a spring with a rest length ($l_0 = 0$). As the springs current length l is greater than l_0, this motor head applies a force which is presented by the blue arrow. In this figure the force applied will not create rotational motion as it is parallel to the filament it is acting on. In figure (b) the two filaments have a smaller angle between them allowing the motor to apply a force, unifying the two filaments. In general, for filaments with an angles of 90^0 between them, the motors need to be at an angle close to 45^0 to both filaments for the force applied to be of any significance.

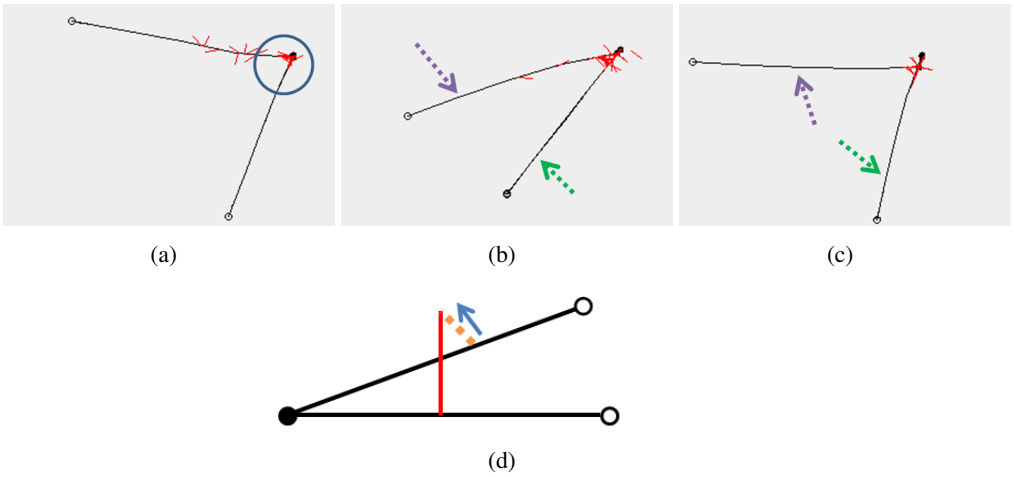

Figure 3.9: Stability of a 90^0 angle. The right angle in fig. (a) is marked by a blue circle. In (b) the angle between the filaments decreases (marked by two dashed arrows), due to attracting forces applied by a large number of motors. In fig. (c) the direction of motion changes abruptly, as the filaments cease to contract and are pushed apart by motorheads applying repulsing forces. These surprising dynamics demand a new explanation in order to comprehend them. Fig. (d) may give a possible explanation. In this shcema two filaments are connected by a motor, with one of the motorheads shown by an orange dashed line. The motor isn't placed between the two filaments rather one of its ends is above the filament, allowing its heads to apply a force expanding the angle between the filaments. Looking carefully at fig. (b), motors of this type (with one end not placed between the two filaments) can be seen, giving credence to this explanation.

The mechanism leading to rotational motion requires certain conditions in order to succeed. First the motor must be able to apply an attracting force on both filaments. Second it needs to apply the force for a substantial amount of time, otherwise it will only cause a minor fluctuation, having no far reaching effects. Filaments with an angle of 90^0 do not seem to fulfill the first requirement, since the force applied by motors creates translational motion (sliding of the two filaments) instead of rotational motion (see fig. 3.8). Another aspect hindering the collapse of 90^0 configurations is the large radial distance between the two filaments. As the motors are non-processive, their ability to apply long term forces is small, meaning that a single motor will usually not manage to move filaments large distances. This is especially true for rotational movement, where motors non-processivity is coupled with the filaments innate stiffness. as a filament on which a motor applied a momentary force, will try to restore its previous state. As 90^0 is a long radial distance and as not all motors can apply substantial attractive forces, 90^0 configurations are quite stable. We noticed yet another factor stabilizing large angles, while analyzing our results. It seems that at times an angle that has started to close can suddenly re-open (see fig. 3.9(a)-3.9(c). This surprising feature seems to be caused by motors with heads outside the area enclosed between the filaments, which pull the filaments outwards (fig. 3.9(d)). To summarize this point, the large radial distance, the motor non-processivity and the restoring forces applied (by the filaments and by the motors) lead to the special stability of 90^0 structures.

The second form of bundles seen are *long bundles*. These are bundles of anti-parallel filaments, joined at their plus ends with their minus ends pointing out in opposite directions (see figure 3.3(g)). The third and probably most interesting form of bundling is of a type we named *deadlock bundles*. In this type of bundle, filaments are anti-parallel but do not undergo polarity sorting, i.e. the motors do not pull the plus ends together while pushing the minus ends out to create a long bundles (see fig. 3.10(a)-3.10(b)). This phenomena seems to stem from a force equilibrium prevailing between the motors leading to a net force of 0 being applied on the filaments (see fig. 3.10(c)). A similar effect has been mentioned by Mogilner *et al*[51], although the case they described included filaments all parallel to each other and motors able to progress along only one of the filaments they were connected to. F. Nédélec has also mentioned a stable anti-parallel overlap [46], but with motors of heterogeneous directionality, i.e some of the motor heads in a motor can move towards the plus end while others can move towards the minus end.

Apart from their difference in appearance and in the dynamics leading to their forma-

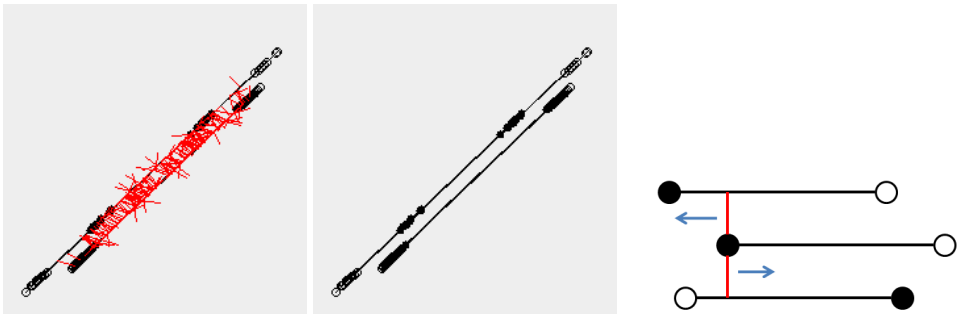

(a) (b) (c)

Figure 3.10: Overlapping anti-parallel filaments connected by motors remaining static despite the many motors connected applying forces on them. Figure (a) shows two bundles connected to each other. When looking at each of these bundles without the motors (b), a fascinating situation is revealed. The lower of the two, has anti-parallel filaments overlapping but their is no pulling of the plus ends towards each other, as usually observed, i.e. in the dynamics leading to long bundles. The same is true for the upper bundle; filaments of opposite polarity are interacting without any observed sorting of polarity. Moreover, the two deadlocked bundles create a super deadlocked bundle, as these two smaller bundles are deadlocked themselves. The schema shown in figure (c) explains this feature. We would like to focus on the forces applied on the middle filament. The upper filament is parallel to the middle one and the motor connecting them is pulling the middle filament left, towards the upper filaments plus end. The lower filament is anti-parallel to the middle filament and the motor connecting them is trying to pull the middle filament right, towards the lower filaments plus end. The sum of forces applied on the middle filament is therefore 0, meaning it will remain static even though forces are being applied on it.

tion, it seems they also vary in their ability to withstand external forces, applied by motors not taking part in the stabilization of the bundle. The least stable type of bundle seems to long bundles, as they are stabilized at one point only, the plus ends of the filaments. Thick bundles seem to be more stable, even though they are also connected at only one point, as a potentially destabilizing motor connecting to the bundle, will probably connect to both filaments, and therefore will not pull the filaments apart. Deadlocked bundles also seem to be the most stable, as they are connected by motors at many points (see 3.10(a)), resulting in a stable bundle, which doesn't disintegrate easily. These deadlocked bundles seem to remain stable even in cases similar to that shown in figure 3.10(b), in which the small bundles making the bigger deadlock bundle are separated allowing a motor to connect to one of the smaller bundles without connecting to the other one.

3.2 Asters

Asters are a "star like" formation, made of filaments with their plus ends all pointing towards the center of the star. In our simulations we found asters to be a common self-organization feature of actin filaments and myosin motors. It seems asters are formed from a V configuration or a long bundle, with many motors at its center. Filaments in the vicinity of this small aggregate, are pulled towards its center and are added to the structure. The additional filament can either unite with one of the filaments in the aggregate, thickening one of the "rays" of the aster, or create a new ray protruding from the aster. Figure 3.11 shows an example of an aster formed by our simulation. An interesting feature to note, is that each neighboring pair of the aster arms has an equal angle between them. This probably occurs because each arm feels an equal force on each side, leading to an equilibrium of forces.

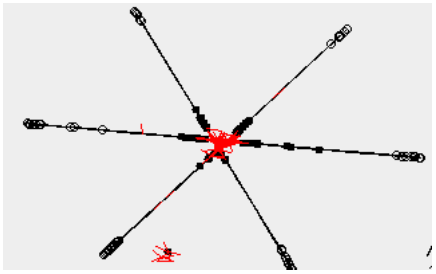

Figure 3.11: An aster with six arms projecting out of its center. Most of the motors are accumulated at the asters center, the location of all of the filaments plus ends. The angle between each pair of arms is similar, probably because the forces applied from each side are comparable, leading to a force equilibrium.

Asters are a stable feature of our system as the motors joining the filaments are at the filaments plus ends, acting in practice as some form of static linkers, since they cannot move from their position at the center of the aster.

The number of arms per aster varies from three to seven arms per aster The most dominant type of aster was a four armed aster, with 90^0 between each neighboring pair of filaments. Moreover, asters with a greater number of arms tended, over time, to collapse into a four armed aster. This feature is illustrated in fig. 3.12, which exhibits a 6 armed aster collapsing into a four armed one. As mentioned in section 3.1, right angles are especially stable due to the large radial distance between the two filaments and due to the decrease in rotational force applied by motors. In addition in an aster there is another cause of stability which is the force equilibrium attained by the equal force felt by each arm from motors on either side. The last condition on its own, isn't enough to promise stability, as asters with more than 4 arms which are equally spaced, may still collapse into a four armed aster. the first two conditions are therefore essential in order to explain the stability of right angled asters. *In-vitro* experiments done by Nedelec [44] and Takiguchi [13] also show that asters arms are not dispersed evenly radiating out in all directions, rather they tend to accumulate, creating thick arms with wide angles between them.

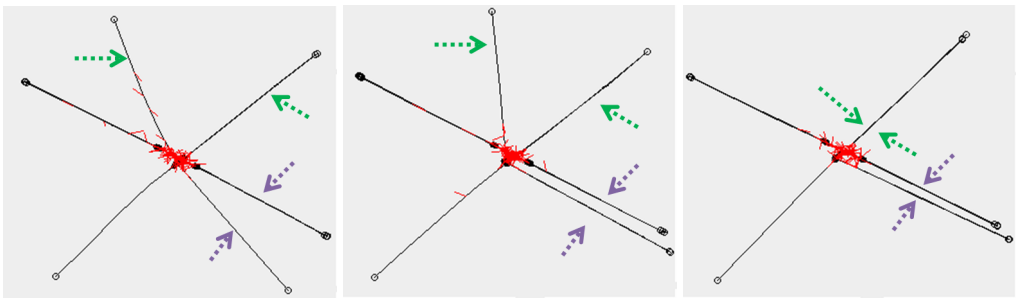

(a) (b) (c)

Figure 3.12: Creation of a four armed right angled aster from an aster with 6 arms. The first pair of arms to collapse is marked by two purple dashed arrows. The second pair of arms to collapse is pointed at by green dashed arrows, leading to the formation of a 4 armed 90^0 aster.

We noticed a special type of aster, one we named *deadlocked aster*. In this kind of aster not all plus ends are concentrated at the asters center, as some of the filaments are deadlocked, preventing polarity sorting from occurring as can be seen in fig. 3.13. This figure also highlights another interesting feature, of filament plus ends which are connected by motors but don't quite meet. We think this is caused by motors positioned between the two filaments, acting as a physical barrier, preventing the two plus ends from meeting.

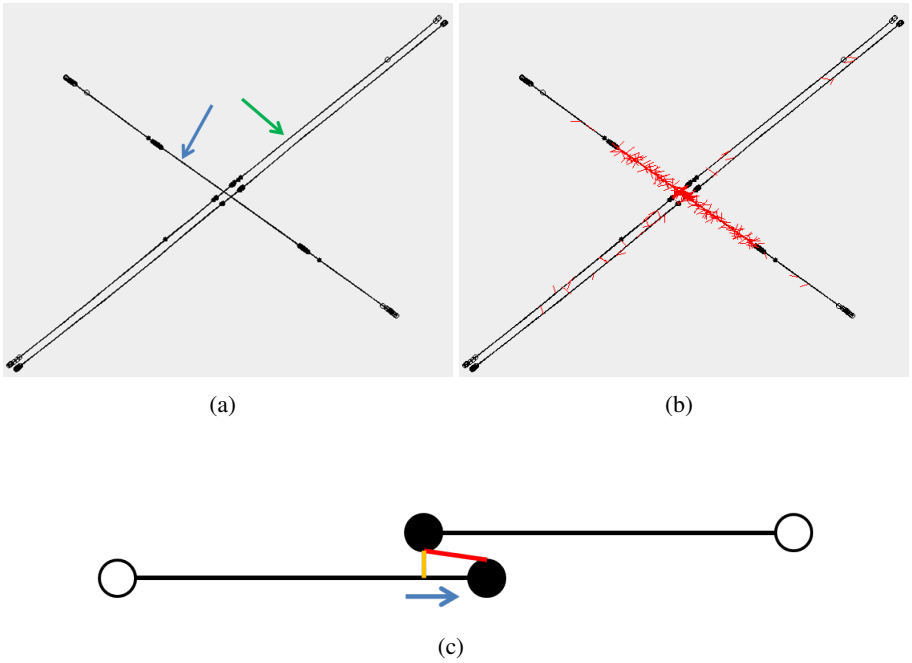

Figure 3.13: Aster of four arms in which not all of the filaments have their plus ends at the center of the aster. Figure (a) shows the filaments without the motors, while (b) shows the same instance of the simulation, this time with the motors (short red rods) visible. The blue arrow in fig. (a) points to a deadlocked bundle participating in the aster. The filament marked by the green arrow has its plus end positioned at the asters center. A close look shows that even this filament doesn't quite reach the center of the aster and this is explained by fig. (c). In this schema two motors are connecting the two bundles; one is colored orange and the other red. The orange motor is applying a force pulling the plus ends of the two filaments together, while the red motor is positioned between the two plus ends, preventing their movement towards each other. Indeed, the distance between the plus end of the filaments (marked by the green arrow in fig. (a)) and the deadlocked bundle (marked by the blue arrow), is approximately the length of a motor (200nm).

3.3 Large Scale Organization

The former sections described small scale features, focusing on the self-organization process of a small group of bundles and motors. These characteristics are barely influenced by changes in the lengths of filaments or by different concentrations of motors and filaments. In contrast large scales features show a great variance depending on lengths and concentrations. Figure 3.14 shows the results of our system after 16 seconds (simulation time), with different concentrations of motors and filaments (fig. 3.14(a)-3.14(c)) and different lengths of filaments (fig. 3.14(d)). These results show that for filaments of the same length (fig. 3.14(a)-3.14(c)) the most important factor is the ratio of motors per filament and not solely the concentration of motors or filaments. Although in all the figures, the number of meta-structures (bundles and asters) stay approximately constant, the number of asters changes, as do the number of free filaments (filaments not part of any meta-structure). For a low ratio of motors per filament (figs. 3.14(a),3.14(c)) the number of asters and free filaments is quite high, while for a high ration of motors per filaments (fig. 3.14(b)) the number of asters and free filaments decreases. Elongating the filaments seems to have a drastic influence on the outcome (fig. 3.14(d)), with the number of meta-structures dropping to one. Another major change is the arrangement of the free filaments. Previously free filaments are seen mingled among the meta structures, while here there are areas with many free filaments containing very few motors. We nicknamed this feature the *balding effect* and it has been previously mentioned [35] as *arrested coarsening*.

To summarize the results: an increase in the number of motors leads to a decrease in the number of asters and free filaments, while leaving the total number of meta-structures constant. An increase in the length of the filaments leads to less meta-structures, and to a balding effect. A summary of the number of asters in each type of simulation can be found in table 3.1.

We would like to propose an explanation for these phenomena. Concerning the effect of motors per filament ratio, an increase in this ratio, means that a larger force is applied, on average, on each filament. Therefore some 90^0 structures may collapse (see fig. 3.15), even though this angle is quite stable. The ratio of motors per filament also affects the number of free filaments in the system, as there are more motors to pull filaments together and incorporate them in bundles or asters. Regarding the influence of filaments length on the outcome, a possible reason may be its effect on the connectivity of the system. When saying a system is connected we imply that a route exists along filaments connected by motors

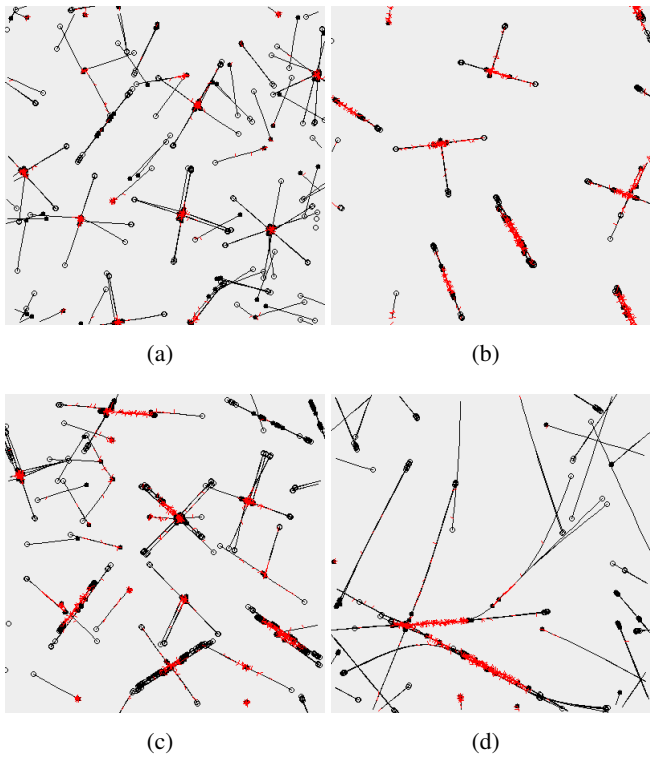

Figure 3.14: Comparison of large scale outcomes as a factor of changes in filament length and concentration and motor concentration. All figures show the results after 16 seconds. Fig. (a) shows the outcome of a simulation with filaments of length 3.2μm, the number of filaments is 240, the number of motors is 1200. This figure shows a large number of asters (8) with varying numbers of arms. Apart from the asters, there are free filaments not bound to any other filament. Fig. (b) presents the result of a simulation in which the concentration of motors was increased. In this simulation there are 2400 motors, changing the ratio of motors per filament from 5 per filament to 10 motors per filament. Here the total number of meta-structures is the same as in fig. (a) but there are nearly no free filaments. Fig. (c) contains 480 filaments each 3.2μm long with 2400 motors, which is a ratio of 5 motors per filament. In this figure the number of meta-structures is still high (9) and like fig. (a) ,which has the same ratio of motors per filament, there are free filaments. Figure (d) has 160 filaments which are 9.6μm long, and 2400 motors. This figure shows only 1 large structure, which encompasses much of the simulated area.

These four figures enable a better understanding of the effect of each of these parameters. Figures (a) and (b) illustrate the influence of motor concentration on the results. High concentrations lead to less free filaments, and cause more collapses of 90^0 asters into bundles. Figures (b), (c) compare different concentrations of filaments. More filaments leads to less collapsing of asters and to more free filaments. Comparing fig. (c) with fig (a) shows similar results even though both the number of filaments and the number of motors are different. The similarity probably stems from the equal ratio of motors per filament in both figures. This points to an interesting observation; the number of filaments or motors does not determine the outcome, rather the ratio of motors per filament. Figures (c), (d) compare different lengths of filaments, showing that longer filaments tend to create less asters, and to leave whole areas of free filaments as opposed to the other figures with free filaments, in which the free filaments were mingled among the meta-structures.

(a) Experiment 1, low concentrations of actin segments

number of segments per filament	4, 240	8, 120	12, 80
5 motors per filament	7.0	—	—
∼10 motors per filament	3.0	2.8	1.2
∼20 motors per filament	—	1.2	0.8

(b) Experiment 2, high concentrations of actin segments

number of segments per filament	4, 480	8, 240	12, 160
5 motors per filament	5.0	—	—
∼10 motors per filament	No data yet	2.0	1.2
∼20 motors per filament	—	1.8	1

Table 3.1: Average number of asters in simulations. Each table deals with different concentrations of filaments. Table (a) shows numbers for low concentrations of filaments. Table (b) shows the average number of asters per simulation for high concentrations of filaments. In both tables, each column header shows the number of segments per filament and the total number of filaments in the system. Each row header shows the number of motors per filament. The value in each box is the average number of asters.

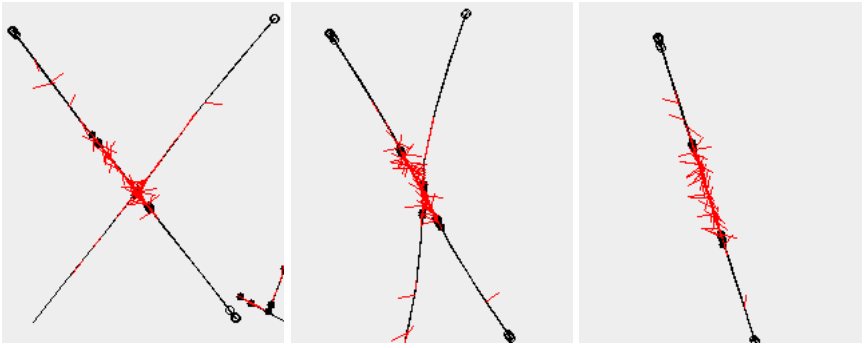

(a) (b) (c)

Figure 3.15: Collapse of right angled aster into a deadlocked bundle. These figures are taken from a simulation containing 240 filaments each 3.2μm long and 2400 motors. Fig. (a) shows an aster with arms at approximately right angles to each other, collapsing (fig. (b)) into a deadlocked bundle (fig. (c)). This figure illustrates that with enough motors, even filaments at right angles may collapse into a bundle.

from any filament to any other filament. If there are no routes along filaments connected by motors (overlapping filaments with no motors connecting them are not counted), the system is not connected. Long filaments, promise a substantial amount of time, in which the system is connected, leaving more time for motors to pull filaments or asters together, leading to a smaller number of independent structures. This explanation is supported by our observations showing that simulations of short filaments become disconnected after 4 seconds, while the connectivity of simulations of long filaments ceases after 12 seconds as can be seen in fig 3.16. It seems that the balding effect which is prominent in systems with long filaments, can also be explained by the difference in connectivity. In inter-connected systems, motors can travel from all parts of the system, to one or two focal points at which all motors concentrate, leaving all other parts devoid of motors. If on the other hand there is no connectivity, the motors are unable to travel outside their local environment, leaving them distributed throughout the system, with no bald areas. Motors cannot usually leave a focal point they have reached as the probability of the motor disconnecting from all filaments it is connected to simultaneously and then diffusing away from the filaments without any of its heads reconnecting is very low, especially as focal points tend to concentrate large numbers of filaments.

Long lasting connectivity also leads to interesting transient states, during the self organization of the filaments. First a mesh is commonly encountered, see 3.16(b). Over time filaments and motors gather, and centers consolidate as shown in fig 3.16(c). These centers also start aggregating (fig. 3.16(d)), resulting in a big aster containing many filaments (fig. 3.16(e)).

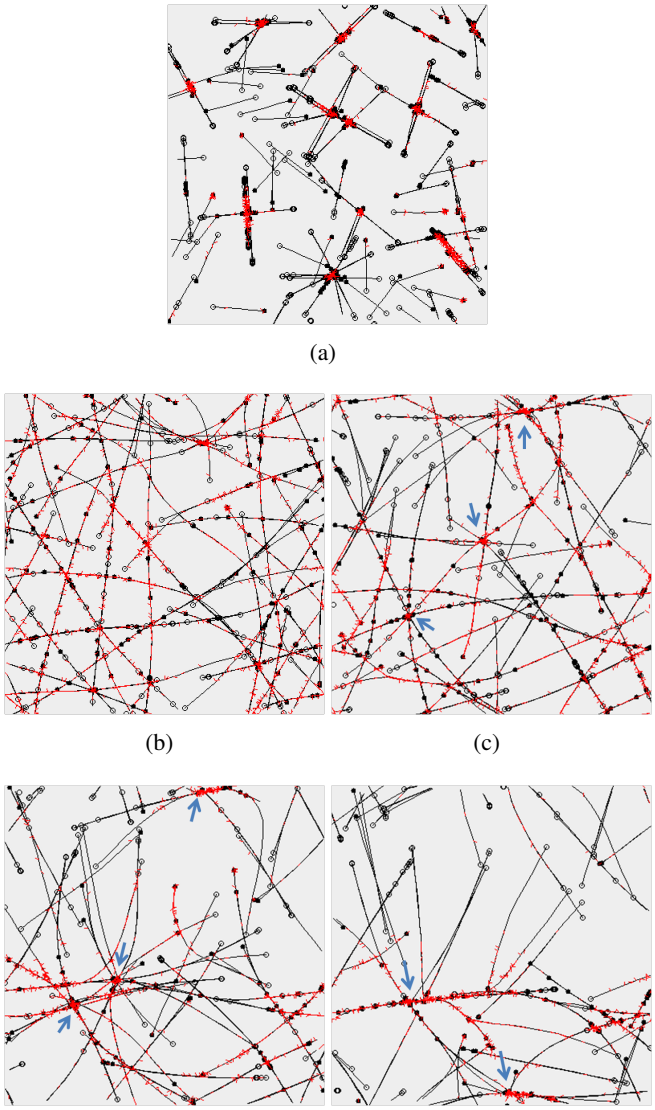

Figure 3.16: Inter-connectivity of filaments. Figure (a) is the configuration after 4 seconds of short filaments 3.2μm long, with a high concentration of actin (480 filaments) and 2400 motors. Figure (b) shows the outcome after the same period of time of a simulation similar in actin concentration and number of motors, but which differs in filament length, with each filament 9.6μm long. These two figures shows great differences in their results, with fig. (a) showing a disconnected system, while fig. (b) exhibits one still highly connected.

Figures (b)-(e) show the major phases in the collapse of a mesh into an aster. Fig. (b) shows the mesh after 4 seconds. Fig. (c) shows the same mesh 2 seconds later, with focal points, marked by blue arrows, starting to emerge. These focal points attract motors and filaments, and can also attract each other as seen in fig. (d), which shows the system after another 2 seconds. In the end, the system converges into an aster, 1.5 seconds later, with a large bald area.

Chapter 4

Summary

The cytoskeleton is a complex system able to self-organize, which includes many members, making it difficult to model. We chose to simulate a simpler system with only filaments and myosin II motors represented explicitly. Our simulation is coarse grained and progresses in time using molecular dynamics. The model used to describe the filaments is a set of nodes connected by springs. Motors are also defined in this way with two central nodes connected by a spring with motor heads radiating from these nodes. These motor heads are the source of most of the dynamics, as they are able to progress along filaments they are bound to. As motor heads originating from the same motor can advance along different filaments, they can cause the filaments to move relative to each other, which gives rise to self-organization.

Our main goals were to study the steady-states formed by our model and acquire a deeper understanding of the dynamics leading to these structures. To this end we executed many simulations in which we chose to keep most properties constant while altering the length of the filaments and the concentration of filaments and motors. The analysis of our results, was done at several different levels. The first stage was analyzing the motion of a single filament, which seems to move in a rather stochastic manner. Second was the self organization of a number of filaments leading to bundles, of three different types: thick bundles, long bundles and deadlocked bundles. The next level was that of asters, where we observed the tendency of arms to collapse leading to 90^0 asters. The widest outlook was at the layout as a whole, where we discovered a correlation between the length of filaments and the number of asters and the appearance of bald areas. We also observed a correlation between the number of motors per filaments and the number of free filaments and the number of asters.

We found deadlocked bundles to be of special interest,first as this form of deadlock

hasn't been previously noted and second as this type of dynamics may provide an explanation for the networks sighted by Backouche *et-al* in [9]. In there work they observed triangular networks which fixated, even though the there were myosin motors in the solute. This is surprising, as the expected dynamics are that the motors should slide the filaments across each other until asters, thick bundles or long bundles are created. We would like to propose that deadlocks occurring inside the network lead to its fixation. An example of a structure incorporating deadlocked bundles can be seen in figure 3.13, where an aster is composed of a deadlocked bundle and a long bundle. It seems the reason we didn't observe this outcome in our system, is that deadlocks demand large amounts of filaments and motors and at the moment we don't have the ability to run such large simulations as the execution time would be on the order of a few years.

Our research is far from finished with many more features to add, and much more analysis of existing data to be done. Regarding filament length, at the moment they are all of an equal length and without the ability to grow and shrink dynamically. A better simulation would probably allow a more varied system with filaments of different length. Moreover the simulation should allow treadmilling, the growth of the filament at its plus end and its shrinking at its minus end. Another parameter which should probably be more variant is the number of motor heads per motor node. Yet another feature, we believe exists and influences the outcome is motor "traffic jams", of many motors moving towards the plus end of a filament, and jamming behind each other. This may have much effect on the outcome, but can't occur in our model, as it doesn't incorporate excluded volume.

Regarding analysis of our results, for the mean time it is mostly qualitative, based mainly on visual analysis of a graphical representation of the output. Some quantitative analysis is necessary, regarding the stochastic nature of our system, the connectivity of our system, and the factors leading to the stability of 90^0 structures.

Other experiments to be carried out regard the effect of motor processivity and filaments stiffness on the outcome, which will allow a better understanding of the differences between the MT-kinesin and actin-myosin systems.

Bibliography

[1] B. Alberts, A. Johnosn, J. Lewis, M. Raff, K. Roberts, and P. Walter. Molecular biology of the cell. Garland Publishing, Inc., New York, NY, USA, fourth edition, 2002.

[2] David Boal. Mechanics of the Cell. Cambridge University Press, January 2002.

[3] Lynne M. Coluccio. Myosins: A Superfamily of Molecular Motors. Springer, December 2007.

[4] T. Kreis and R. Vale. Guidebook to the cytoskeletal and motor proteins. Guide book series., 1993.

[5] S. Yamashiro-Matsumura and F. Matsumura. Intracellular localization of the 55-kD actin-bundling protein in cultured cells: spatial relationships with actin, alpha-actinin, tropomyosin, and fimbrin. Journal of Cell Biology, 103(2):631–640, 1986.

[6] R.J. Pelham and F. Chang. Actin dynamics in the contractile ring during cytokinesis in fission yeast. Nature, 419(6902):82–86, 2002.

[7] J.Q. Wu and T.D. Pollard. Counting cytokinesis proteins globally and locally in fission yeast. Science, 310(5746):310–314, 2005.

[8] A.B. Verkhovsky, T.M. Svitkina, and G.G Borisy. Polarity sorting of actin filaments in cytochalasin treated fibroblasts. Journal of Cell Science, 110:1693–1704, 1997.

[9] F. Backouche, L. haviv, D. Groswasser, and A. Bernheim-Groswasser. Active gels: dynamics of patterning and self-organization. Physical Biology, 2006.

[10] G.G. Borisy, D.W. Cleveland, and D.B. Murphy. Molecular biology of the cytoskeleton. Cold Spring Harbor Laboratory, 1984.

[11] Jonathan Howard. Mechanics of Motor Proteins and the Cytoskeleton. Sinauer Associates, Inc, first edition, 2001.

[12] R. Urrutia, MA McNiven, JP Albanesi, DB Murphy, and B. Kachar. Purified kinesin promotes vesicle motility and induces active sliding between microtubules in vitro. Proceedings of the National Academy of Sciences, 88(15):6701–6705, 1991.

[13] Yohko Tanaka-Takiguchi, Toshihito Kakei, Akinori Tanimura, Aya Takagi, Makoto Honda, Hirokazu Hotani, and Kingo Takiguchi. The elongation and contraction of actin bundles are induced by double-headed myosins in a motor concentration-dependent manner. Journal of Molecular Biology, 341(2):467 – 476, 2004.

[14] T. Surrey, F. Nedelec, S. Leibler, and E. Karsenti. Physical properties determining self-organization of motors and microtubules. science, 292, 2001.

[15] Kingo Takiguchi. Heavy meromyosin induces sliding movements between antiparallel actin filaments. Journal of Biochemistry, 109:520–527, 1991.

[16] F. Pampaloni, G. Lattanzi, A. Jonáš, T. Surrey, E. Frey, and E.L. Florin. Thermal fluctuations of grafted microtubules provide evidence of a length-dependent persistence length. Proceedings of the National Academy of Sciences, 103(27):10248, 2006.

[17] F. Gittes, B. Mickey, J. Nettleton, and J. Howard. Flexural rigidity of microtubules and actin filaments measured from thermal fluctuations in shape. Journal of Cell Biology, 120(4):923–934, 1993.

[18] Joe Howard. Molecular motors: structural adaptation to cellular functions. Nature, 389:561–7, Oct 1997.

[19] Hatsumi Nakazawa and Ken Sekimoto. Polarity sorting in a bundle of actin filaments by two-headed myosins. Journal of the Physical Society of Japan, 65(8):2404–2407, 1996.

[20] Ken Sekimoto and Hatsumi Nakazawa. Contraction of a bundle of actin filaments: 50 years after szent-gyorgyi, 1998.

[21] K. Kruse and F. Jülicher. Actively contracting bundles of polar filaments. Phys. Rev. Lett., 85(8):1778–1781, Aug 2000.

[22] K. Kruse, S. Camalet, and F. Jülicher. Self-propagating patterns in active filament bundles. Phys. Rev. Lett., 87(13):138101, Sep 2001.

[23] Tanniemola B. Liverpool and M. Cristina Marchetti. Organization and instabilities of entangled active polar filaments. Physical Review Letters, 90:138102, 2003.

[24] T. B. Liverpool and M. C. Marchetti. Liverpool and marchetti reply:. Phys. Rev. Lett., 93(15):159802, Oct 2004.

[25] F. Jlicher, K. Kruse, J. Prost, and J.-F. Joanny. Active behavior of the cytoskeleton. Physics Reports, 449(1-3):3 – 28, 2007. Nonequilibrium physics: From complex fluids to biological systems III. Living systems.

[26] T.B. Liverpool. Active gels: where polymer physics meets cytoskeletal dynamics. Philosophical Transactions of the Royal Society A: Mathematical, Physical and Engineering Sciences, 364(1849):3335–3355, 2006.

[27] B. Bassetti, M. Cosentino Lagomarsino, and P. Jona. A model for the self-organization of microtubules driven by molecular motors. The European Physical Journal B-Condensed Matter and Complex Systems, 15(3):483–492, 2000.

[28] R. Aditi Simha and Sriram Ramaswamy. Hydrodynamic fluctuations and instabilities in ordered suspensions of self-propelled particles. Phys. Rev. Lett., 89(5):058101, Jul 2002.

[29] K. Kruse, J. F. Joanny, F. Jülicher, J. Prost, and K. Sekimoto. Asters, vortices, and rotating spirals in active gels of polar filaments. Phys. Rev. Lett., 92(7):078101, Feb 2004.

[30] K. Kruse, JF Joanny, F. J

"ulicher, J. Prost, and K. Sekimoto. Generic theory of active polar gels: a paradigm for cytoskeletal dynamics. The European Physical Journal E: Soft Matter and Biological Physics, 16(1):5–16, 2005.

[31] Y. Hatwalne, S. Ramaswamy, M. Rao, and R.A. Simha. Rheology of active-particle suspensions. Physical review letters, 92(11):118101, 2004.

[32] F. Ziebert and W. Zimmermann. Comment on Instabilities of isotropic solutions of active polar filaments. Physical review letters, 93(15):159801, 2004.

[33] A. Ahmadi, T. B. Liverpool, and M. C. Marchetti. Nematic and polar order in active filament solutions. Phys. Rev. E, 72(6):060901, Dec 2005.

[34] Igor S. Aranson and Lev S. Tsimring. Pattern formation of microtubules and motors: inelastic interaction of polar rods. Physical Review E, 71:050901, 2005.

[35] Ha Youn Lee and Mehran Kardar. Macroscopic equations for pattern formation in mixtures of microtubules and motors. Physical Review E, 64:0561131, 2001.

[36] S. Sankararaman, G.I. Menon, and PB Sunil Kumar. Self-organized pattern formation in motor-microtubule mixtures. Physical Review E, 70(3):31905, 2004.

[37] V Tozzini. Coarse-grained models for proteins. CURRENT OPINION IN STRUCTURAL BIOLOGY, 15(2):144–150, APR 2005.

[38] M Muller and LG MacDowell. Interface and surface properties of short polymers in solution: Monte Carlo simulations and self-consistent field theory. MACROMOLECULES, 33(10):3902–3923, MAY 16 2000.

[39] K Binder, A Milchev, and J Baschnagel. Simulation studies on the dynamics of polymers at interfaces. ANNUAL REVIEW OF MATERIALS SCIENCE, 26:107–134, 1996.

[40] Peter J. Bond, John Holyoake, Anthony Ivetac, Syma Khalid, and Mark S. P. Sansom. Coarse-grained molecular dynamics simulations of membrane proteins and peptides. JOURNAL OF STRUCTURAL BIOLOGY, 157(3):593–605, MAR 2007.

[41] Maddalena Venturoli, Maria Maddalena Sperotto, Marieke Kranenburg, and Berend Smit. Mesoscopic models of biological membranes. PHYSICS REPORTS-REVIEW SECTION OF PHYSICS LETTERS, 437(1-2):1–54, DEC 2006.

[42] PV Coveney and PW Fowler. Modelling biological complexity: a physical scientist's perspective. JOURNAL OF THE ROYAL SOCIETY INTERFACE, 2(4):267–280, SEP 22 2005.

[43] F.J. Nedelec, T. Surrey, A.C. Maggs, and S. Leibler. Self-organization of microtubules and motors. nature, 389, 1997.

[44] F. Nedelec and T. Surrey. Dynamics of microtubule aster fromation by motor complexes. Physics at the scale of the cell, 2001.

[45] Clifford P. Brangwynne, Gijsje H. Koenderink, Frederick C. MacKintosh, and David A. Weitz. Cytoplasmic diffusion: molecular motors mix it up. J. Cell Biol., 183(4):583–587, 2008.

[46] F. Nedelec. Computer simulations reveal motor peroperties generating stable antiparallel microtubule interactions. The Journal of Cell Biology, 158(6):1005–1015, 2002.

[47] L.D. Landau and E.M. Lifshitz. Theory of Elasticity, Course of Theoretical Physics vol 7. VII, 3rd revised edition (Butterworth-Heinemann, London), 1995.

[48] Daisuke Mizuno, Catherine Tardin, C. F. Schmidt, and F. C. MacKintosh. Nonequilibrium Mechanics of Active Cytoskeletal Networks. Science, 315(5810):370–373, 2007.

[49] B. Kachar. Polarity and velocity of sliding filaments: control of direction by actin and of speed by myosin. Science, 249(4967):406–408, 1990.

[50] Karsten Kruse and Frank Jülicher. Self-organization and mechanical properties of active filament bundles. Phys. Rev. E, 67(5):051913, May 2003.

[51] Assaf Zemel and Alex Mogilner. Motor-induced sliding of microtubule and actin bundles. Phys. Chem. Chem. Phys., 2009.